GIScience & Remote Sensing

ISSN: (Print) (Online) Journal homepage: www.tandfonline.com/journals/tgrs20

Spatiotemporal analysis of tropical vegetation ecosystems and their responses to multifaceted droughts in Mainland Southeast Asia using satellite-based time series

Tuyen V. Ha, Soner Uereyen & Claudia Kuenzer

To cite this article: Tuyen V. Ha, Soner Uereyen & Claudia Kuenzer (2024) Spatiotemporal analysis of tropical vegetation ecosystems and their responses to multifaceted droughts in Mainland Southeast Asia using satellite-based time series, GIScience & Remote Sensing, 61:1, 2387385, DOI: 10.1080/15481603.2024.2387385

To link to this article: https://doi.org/10.1080/15481603.2024.2387385

Published online: 05 Aug 2024.

GISCIENCE & REMOTE SENSING
2024, VOL. 61, NO. 1, 2387385
https://doi.org/10.1080/15481603.2024.2387385

Taylor & Francis
Taylor & Francis Group

Spatiotemporal analysis of tropical vegetation ecosystems and their responses to multifaceted droughts in Mainland Southeast Asia using satellite-based time series

Tuyen V. Ha[a,b,c], Soner Uereyen[a] and Claudia Kuenzer[a,b]

[a]German Remote Sensing Data Center, German Aerospace Center, Wessling, Germany; [b]Institute of Geography and Geology, University of Wuerzburg, Wuerzburg, Germany; [c]Faculty of Resources Management, Thai Nguyen University of Agriculture and Forestry, Thai Nguyen, Vietnam

ABSTRACT

Drought ranks among the costliest of all climate-related phenomena and manifests in various forms, posing significant challenges in understanding its influence on agriculture and natural ecosystems. Mainland Southeast Asia (MSEA), a significant region of tropical agriculture and vegetation ecosystems, has become increasingly susceptible to drought hazards. In this study, we characterized and assessed vegetation dynamics and their drought impacts using correlation analysis and explainable machine learning methods under different vegetation types and elevation zones during the dry growing seasons from 2000 to 2022. Specifically, we characterized the vegetation dynamics and their trend in space and time. Next, we assessed vegetation-drought responses in consideration of meteorological, hydrological, and agricultural droughts under different land cover types and elevation characteristics. Lastly, we used an explainable machine learning method to quantify the drivers and impacts of multifaceted droughts on natural and undisturbed vegetation ecosystems. Our findings revealed that nearly 70% of the MSEA region experienced a greening trend despite large areas of vegetative damage during the drought years. Vietnam witnessed increasing vegetation condition in most observed years while the declining trend was mainly found in Cambodia and southern Laos. Vegetation-drought responses showed that tropical vegetation had a high sensitivity to drought conditions, and stronger responses were observed in rainfed crop, mixed forest, and deciduous forest at lower altitude areas. In natural and undisturbed ecosystems, short-term meteorological and agricultural drought disturbances accounted for nearly 93% of variations in tropical vegetation. Among the different examined drought indices, the 3-month Standardized Precipitation Evapotranspiration (SPEI-3) and Temperature Condition Index (TCI) were identified as the factors having the largest influence, together explaining about 55% of the observed natural undisturbed vegetation variations. These findings deepen our understanding of tropical vegetation-drought responses and the underlying drivers of natural and undisturbed ecosystems. Such insights could provide valuable information to assist national and local governments in the MSEA region in developing effective drought management and adaptation programs to safeguard tropical agricultural production and natural ecosystems amidst growing climate challenges.

ARTICLE HISTORY
Received 19 February 2024
Accepted 27 July 2024

KEYWORDS
Undisturbed ecosystems; drivers; remote sensing; earth observation, SHAP; random forest

Introduction

Drought is a persistent phenomenon reoccurring in most climatic zones and ranks among the costliest of all climate-related hazards (Ha et al. 2022; Masson-Delmotte et al. 2021). The primary cause of drought stems from a lack of precipitation against the long-term average, and it can be grouped into four main types: meteorological, agricultural, hydrological, and socio-economic droughts (A. K. Mishra and Singh 2010; Q. Zhao et al. 2023). Each of these types entails different consequences and temporal aspects, contributing to the multifaceted impacts of drought on agricultural, natural vegetation, and human systems (P. Wang et al. 2022; West, Quinn, and Horswell 2019). For example, meteorological drought usually initiates with a lack of precipitation and/or higher temperatures over a short period (e.g. 1–3 months) (A. K. Mishra and Singh 2010). By contrast, hydrological drought evolves from an extended deficit in precipitation (e.g. more than six months), resulting in reduced surface water bodies and groundwater (A. K. Mishra and Singh 2010). Agricultural drought,

CONTACT Soner Uereyen soner.uereyen@dlr.de

closely linked to meteorological and hydrological droughts, manifests through depleted soil moisture levels, directly impacting agrarian productivity (Ha et al. 2022; A. K. Mishra and Singh 2010). With ongoing global warming crises, drought is projected to intensify and become more frequent and devastating in many parts of the world (IPCC (2013); Masson-Delmotte et al. 2021), including the Mainland Southeast Asia (MSEA) region.

Vegetation is a fundamental element of terrestrial ecosystems and is crucial in safeguarding global biodiversity, hydrological cycles, climate regulations, and food supplies (Qin et al. 2021). However, climate change and human disturbances have posed significant threats to natural ecosystems (Anderegg, Kane, and Anderegg 2013; Qi et al. 2023; H. Wang et al. 2015) and social/human health (Patz et al. 2005; Smith et al. 2014). Droughts are identified as having the most direct and widespread impact on agriculture (Sun et al. 2023; Venkatappa et al. 2021) and ecosystem function (Cao et al. 2023). For example, the annual loss of European agriculture due to drought-related events amounts to $9 billion, which could exceed $65 billion by the year 2100 (Naumann et al. 2021). This figure for the MSEA region is estimated to be $19 billion per year (UNESCAP 2019). Also, recent studies reSported droughts causing both widespread vegetation damage and forest mortality across Europe (Obladen et al. 2021; Senf et al. 2020), Australia (De Kauwe et al. 2020; Qin et al. 2022), China (Fang et al. 2019; H. Wang et al. 2015), and the MSEA region (Fan et al. 2023; Ha, Uereyen, and Kuenzer 2023; B. Zhang et al. 2014). For instance, Senf et al. (2020) estimated nearly 500 thousand ha of European forest mortality being caused by drought events from 1987 to 2016. Apart from drought-related factors, human-induced activities also significantly influence vegetation growth, both positive and negative. For example, shifting agriculture and deforestation damaged vegetation in Laos and Cambodia (Chen et al. 2023, Namkhan et al. 2021), while forest plantation programs significantly increased greening in Vietnam (Nambiar 2021).

Due to the effects of the ongoing climate crisis together with unprecedented human activities, it has become increasingly crucial to understand how vegetation reacts to a spectrum of natural and human-induced influences and their underlying determinants. Recent progress in remote sensing and numerical modeling has facilitated the open accessibility of extensive satellite-derived time series and reanalysis datasets (AghaKouchak et al. 2015; Muñoz-Sabater et al. 2021), such as Moderate Resolution Imaging Spectroradiometer (MODIS) and ERA5-Land products. Such open data policies have fueled the growing number of drought-vegetation studies (AghaKouchak et al. 2015; Ha et al. 2022; A. K. Mishra and Singh 2010; West, Quinn, and Horswell 2019). Several drought indices have been widely accepted to characterize different aspects of drought conditions and their impacts on vegetation, including the most commonly used Standardized Precipitation Index (SPI) (McKee, Doesken, and Kleist 1993), Standardized Precipitation Evapotranspiration Index (SPEI) (Vicente-Serrano, Beguería, and López-Moreno 2010), Temperature Condition Index (TCI) (Kogan 1995), Soil Water Deficit Index (SWDI) (A. Mishra et al. 2017), and Palmer Drought Severity Index (PDSI) (Palmer 1965). Among the existing methods, spatiotemporal correlation analysis was probably the most widely used to evaluate vegetation growth sensitivities to droughts across different climatic regions (Jin et al. 2023; Xu et al. 2018; X. Zhang and Zhang 2019). Such relationships are typically established based on single drought and vegetation indices (e.g. NDVI: Normalized Difference Vegetation Index, EVI: Enhanced Vegetation Index). Specifically, most recent studies estimated vegetation-drought sensitivities using NDVI time series together with SPEI/SPI observations (Cao et al. 2023; Jin et al. 2023; Xu et al. 2018) and other comparable combined indices (X. Zhang and Zhang 2019; B. Zhang et al. 2014).

However, vegetation dynamics are complex and influenced by numerous drought-related factors, each with its unique impact on vegetation growth. For instance, the SWDI offers crucial insights into vegetation responses to transient soil moisture deficits (A. Mishra et al. 2017). Conversely, the multi-timescale SPEI and SPI delve into the sensitivities of vegetation to different short-term and long-term climate-driven drought events (Jin et al. 2023; H. Wang et al. 2015). Gaining insights into the multifaceted aspects of vegetation-drought associations is essential for assessing different drought-related risks and enhancing drought mitigation and adaptation strategies. In addition, while correlation analysis offers great insights into spatiotemporal vegetation-drought

relationships, it may struggle to discover the potential underlying drivers of change on vegetation ecosystems. In this regard, robust and explainable machine learning techniques are required in addition to traditional correlation analyses to address these challenges. Despite the growing interest in explainable machine learning, such methods received little attention in vegetation-drought studies (B. Zhang et al. 2023).

The MSEA is a major region of tropical agriculture and biodiversity ecosystems worldwide, but has become increasingly vulnerable to droughts and human-induced activities over the past two decades. Drought events mainly occur in this region during the dry growing seasons and have caused devastating damage to agriculture and natural ecosystems. For instance, a recent Vegetation Condition Index (VCI) analysis revealed that vegetation suffered from a significant decline during the dry seasons in 2004, 2005, 2010, 2016, 2019, and 2020 across the MSEA region (Ha, Uereyen, and Kuenzer 2023). Likewise, Son et al. (2012) employed the vegetation temperature dryness index and found larger drought-induced crop areas in Cambodia and Thailand. Also, B. Zhang et al. (2014) reported a significant reduction in vegetation productivity in 2005 and 2010 in the Mekong Basin using the Gross Primary Productivity (GPP). Notably, Fan et al. (2023) examined the influence of anthropogenic and climatic factors on vegetation greening using a partial correlation analysis and identified temperature and precipitation as most impactful. Although these studies provide great insights into vegetation variations, understanding the multifaceted dimensions of vegetation-drought responses and the driving factors of natural undisturbed vegetation ecosystems in the region remain understudied. For example, our prior study employed MODIS-based time series to explore vegetation-related drought characteristics, including trends (Ha, Uereyen, and Kuenzer 2023). The study highlighted that drought frequently occurred in this region during the dry seasons over the past decades. However, it lacked comprehensive insights into how vegetation responds to droughts and how these trends vary across different land cover types and elevations.

In this study, we present an in-depth analysis of tropical vegetation dynamics and their multifaceted drought impacts using MODIS-based vegetation time series and multi-temporal and multi-type drought indices during the dry growing seasons from 2000 to 2022 in the MSEA region. Specifically, we first examined tropical vegetation dynamics and their trend across the study region. Secondly, we evaluated the responses of vegetation to drought using multifaceted drought indices in consideration of various land cover types and elevation characteristics. Finally, we quantified the drivers of natural and undisturbed vegetation dynamics (e.g. vegetation ecosystems without significant human disturbances) to multifaceted drought indices using a robust and explainable machine learning method. The findings of this study will contribute to a better understanding of tropical vegetation responses and the underlying drivers of natural ecosystem change related to different droughts in the MSEA region. Such insights, in turn, could offer valuable support for developing effective drought management and adaptation strategies in safeguarding food security and tropical ecosystems amidst growing global climate-related challenges.

Study area and materials

Study region

The MSEA region is located in Southeast Asia, and it extends over five different countries with a total landmass of nearly 2 million km^2 (Figure 1). The geography of this region is characterized by different land cover types (Figure 1(a)) and diverse elevations (Figure 1(b)). Here, we reclassified the MSEA land surface into seven major types: rainfed cropland, irrigated cropland, shrubland, mixed forest, evergreen forest, deciduous forest, and other non-vegetation (e.g. water, bare-land, and built-up structures) using the European Space Agency (ESA) Climate Change Initiative (CCI) land cover product (Santoro et al. 2017). In this region, cropland and forest are two dominant land cover types, accounting for nearly 80% of the landmass. Rainfed croplands and evergreen forests have the largest share, with nearly 35% and 26%, respectively (inset plot in Figure 1(a)). Rainfed croplands are largely found in Thailand (~55%), Myanmar (~26%) and Cambodia (~37%), whereas irrigated agriculture (e.g. rice crop) is mainly observed in the Vietnamese Lower Mekong Delta.

The MSEA region falls within tropical and subtropical zones (here referred to as tropical) as the

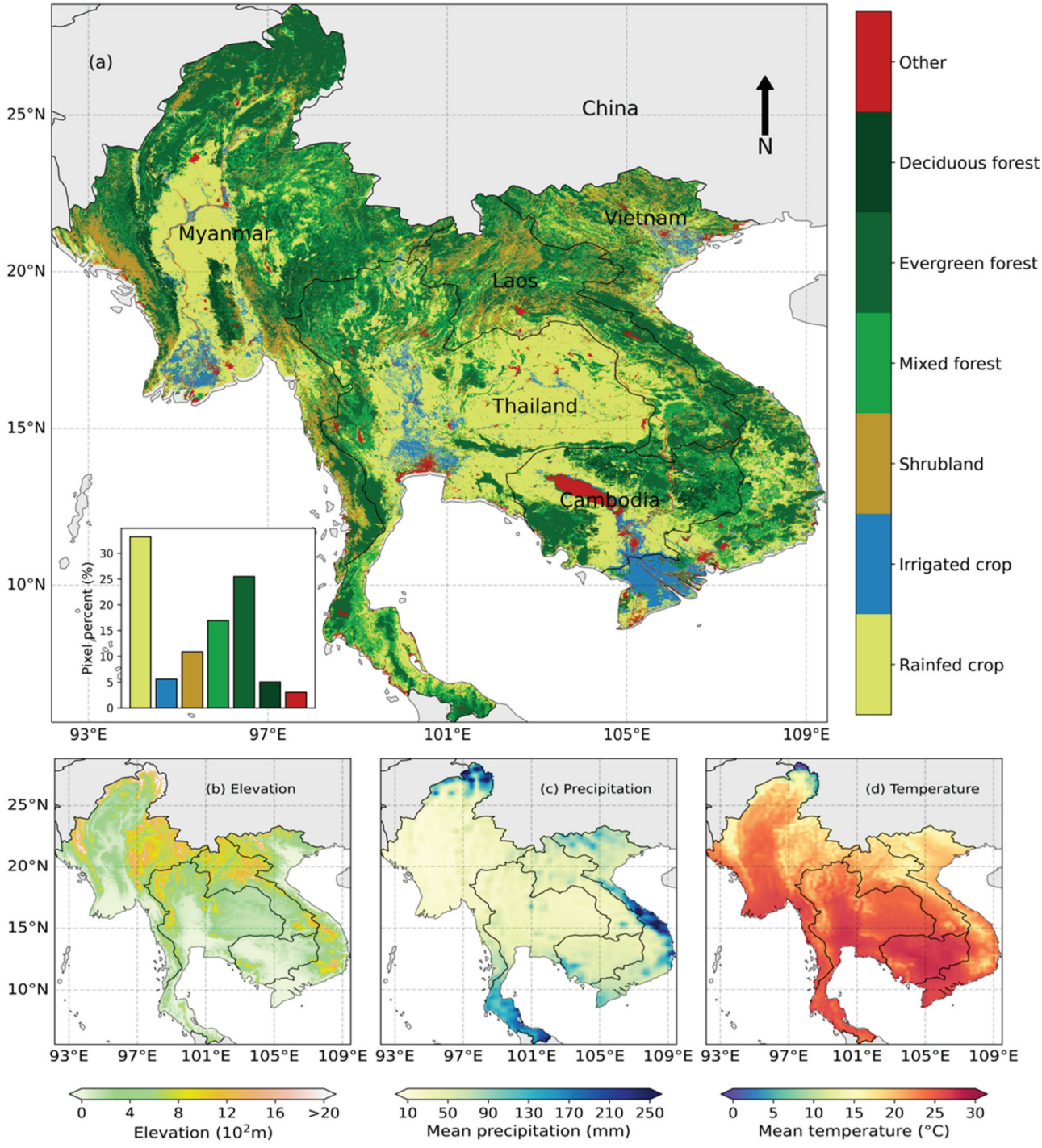

Figure 1. Map of the MSEA countries with different land cover classes (a) from the ESA CCI land cover product. The land cover types are reclassified into 7 major classes using the ESA CCI land cover dataset, and the sub-bar plot indicates the pixel percentage of seven land cover classes, respectively. The below maps show topographical characteristics (b) mean total precipitation (c) and mean temperature (d) during the dry seasons (November-April) from 2000 to 2022.

subtropical climate covers a small portion and can be found only in some high-altitude mountains in northern Myanmar (Beck et al. 2018; Köppen 1936). Overall, seasonal and tropical monsoon climate conditions primarily characterize weather patterns in this region (Yishan et al. 2022). Despite some climate variations across the MSEA countries, there are two main climate seasons: the rainy and dry seasons, each accompanied by two corresponding growing seasons. The rainy season frequently suffers from heavy precipitation,

for example in Vietnam (~400 mm/month) due to the southwest monsoon, spanning from May to October. However, the dry season experiences a significant reduction in precipitation (from November to April), leading to frequent drought conditions and heat waves across the region (Ha, Uereyen, and Kuenzer 2023; Singh and Qin 2020). ERA5-Land data showed that most of the region suffers from the least rainfall, with less than 15 mm/month (Figure 1(c)), except the coastal areas of Vietnam, and high temperatures during the dry season (Figure 1(d)). Higher temperatures are dominantly observed in the southern region, especially in Cambodia and Vietnamese Lower Mekong Delta. The average temperatures in these areas during the dry season are around 30°C, while the northern region had lower temperature, especially in the high mountains of Myanmar (Figure 1(d)).

Datasets and pre-processing

This study employed a wide array of geospatial datasets, including MODIS NDVI and land surface temperature (LST) measurements, ERA5-Land reanalysis products, ESA CCI land cover, digital elevation model (DEM), soil property information as well as the World Database on Protected Areas (WDPA). All adopted datasets, except for the WDPA and ESA CCI land cover, were accessed through the Google Earth Engine (GEE) cloud computing platform (Gorelick et al. 2017), and they were converted into a geographic coordinate system (WGS84) and resampled to 1 km spatial resolution. In this study, the NDVI time series was used to derive the VCI, an indicator of vegetation health condition (Section 3.1.1). The ERA5-Land reanalysis, soil properties, and MODIS LST datasets were used to calculate different drought indices (Section 3.1.2), while the WDPA was used to define the natural and undisturbed vegetation areas (Section 3.2.3). A concise description of each dataset used in this study is provided in Table 1 and elaborated upon in the subsequent sections.

Modis-based NDVI and LST time series

This study used analysis-ready vegetation-based time-series measurements from both Terra and Aqua MODIS NDVI 16-day 1-km spatial resolution products (version 6.1) from 2000 to 2022. This dataset has been generated from georeferenced, radiometrically, and atmospherically corrected MODIS red and near-infrared reflectance bands (Didan 2021). The 16-day product was derived by selecting the highest-quality daily NDVI pixels acquired over the course of a 16-day period. Here, we used the MODIS-associated quality assurance band (QA) within the GEE platform to mask out cloud-related pixels. In case of missing NDVI observations, we applied linear interpolation, and monthly composites were subsequently generated using the median value composite (MVC) technique (Ha, Uereyen, and Kuenzer 2023), known for its robustness in handling outliers (Göttsche and Olesen 2001). Next, the Savitzky-Golay method was undertaken to reconstruct the MODIS NDVI time-series measurements, reflecting a more reliable vegetation growth curve (De Jong et al. 2011; Ha, Uereyen, and Kuenzer 2023). Finally, this dataset was reprojected into a geographic coordinate system (WGS84) from the Sinusoidal grid system and restricted to the MSEA region at 1 km spatial resolution.

The LST was obtained from Terra and Aqua daytime MODIS 8-day 1 km spatial resolution (version 6.1) from 2000 to 2022 (Wan, Hook, and Hulley 2021). Here, cloud-covered LST pixels were removed from the MODIS LST collection before monthly composites

Table 1. Description of satellite and reanalysis datasets used in this study. The data period indicates the timeframe during which the data was generated or last updated.

Datasets/sensors	Variables	Temporal resolution	Spatial resolution	Data period	Source
MODIS	NDVI and LST	16/8-day	1 km	2000 - present	Didan (2021) and Wan, Hook, and Hulley (2021)
ERA5-Land	Precipitation, soil moisture, air temperature, net radiation, wind, humidity	Hourly	~10 km	1950 - present	Muñoz-Sabater et al. (2021)
Open soil data	Carbon organic, clay, and sand contents	–	250 m	2018	Hengl (2018)
ESA CCI land cover	Land cover/land use	Yearly	300 m	2000–2020	Santoro et al. (2017)
SRTM DEM	Digital elevation model	–	90 m	2000	Berry, Garlick, and Smith (2007)
World Database Protected Areas (WDPA)	Terrestrial protected areas	–	–	2023	IUCN and UNEP (2020)

were retrieved using the mean composite method. Missing LST observations were interpolated based the nearest neighbor pixels. This dataset was transformed into a geographical coordinate system (WGS84) and subsequently limited to the MSEA region.

Climate and soil reanalysis products

ERA5-Land is the fifth-generation reanalysis product, developed by the European Center for Medium-Range Weather Forecasts (ECMWF), providing consistent, multi-temporal, and high-resolution meteorological and land surface information from 1950 to the present, with a global coverage at 9 km spatial resolution. This dataset was produced from a combination of station-based observation data and state-of-the-art atmospheric-land assimilation and numerical modeling techniques (Muñoz-Sabater et al. 2021). The ERA5-Land variables have undergone extensive regional- and global-scale validation in recent years. For example, Muñoz-Sabater et al. (2021) revealed that the ERA5-land soil moisture had good agreement with in-situ soil observations from 2010 to 2018 globally, while Rivoire, Martius, and Naveau (2021) found strong agreement between ERA5-Land variables and station-based data across European countries. These validations demonstrated the reliability and accuracy of ERA5-Land data in capturing essential climatic and environmental variables.

For this study, we selected soil moisture content and meteorological variables from the ERA5-Land hourly dataset between 2000 and 2022. The hourly climate variables were first aggregated into daily observations, and these daily measurements were then used to calculate potential evapotranspiration (PET) based on the FAO-56 Penman-Monteith approach (Allen et al. 1998) using the pyet Python package (Vremec, Collenteur, and Birk 2023). The PET data serves as a key input component for deriving climate-based drought indices such as the SPEI. After the PET calculation, we selected three variables, namely PET, precipitation and soil moisture. These variables were aggregated monthly for later calculating the SPEI, SPI, and SWDI (Section 3.1.2). These monthly datasets were resampled to 1 km to align with the spatial resolution of the MODIS product using the bilinear method.

Land cover data

Numerous global land cover products are available at different spatial and temporal resolutions. In this study, the ESA CCI land cover dataset with 300 m resolution was used. The advantages of this data are its consistency, comparatively high-spatial resolution, improved accuracy, and annual update. This dataset has been curated by harnessing high-quality multi-satellite products, such as SPOT, MERIS, and PROBA-V, utilizing a blend of state-of-the-art machine learning algorithms (Santoro et al. 2017). Furthermore, every pixel in this dataset was consistently cross-verified with several-year observations to minimize potential classification errors. For this study, we sourced annual land cover maps, spanning the years 2000 to 2020 from the ESA CCI land cover program (https://www.esa-landcover-cci.org/). Subsequently, we selected unchanged vegetation pixels over the past two decades covering the MSEA region and categorized into six main types: rainfed cropland, irrigated cropland, mixed forest, evergreen forest, deciduous forest, and shrubland. In order to ensure the compatibility with MODIS products, we aggregated the land cover data to a spatial resolution of 1 km using the nearest neighbor method.

Auxiliary variables

This study also used the World Protected Area Database, elevation, and soil property datasets to facilitate the further analysis. The World Database on Protected Areas, developed jointly by the UN Environment Program and the International Union for Conservation of Nature, offers a comprehensive and up-to-date source of information on global protected areas, such as national parks, wildlife reserves, and marine protected areas. Here, this dataset was used to define the natural and undisturbed vegetation ecosystems, which serves the driver analysis of natural vegetation change in the Section 3.2.3. We selected only terrestrial protected areas within the MSEA region, resulting in a total of 417 natural (protected) areas. On average, the terrestrial protected areas in Laos and Cambodia had the largest area, ~160 thousand and ~ 115 thousand hectares, respectively, while Vietnam featured the smallest, ~32 thousand hectares. This dataset contains multi-part geometries and some overlapping polygons, so we decomposed these multi-part geometries into individual single-part polygons and selected only the

protected areas that exceeded 4 MODIS pixels (~400 hectares), leading to a selection of 421 protected polygons. In addition, we accessed the Shuttle Radar Topography Mission (SRTM) elevation data through the GEE platform. This dataset provides consistent and high-quality near-global extent elevation at 90 m spatial resolution (Berry, Garlick, and Smith 2007). Finally, we retrieved the characteristics of top-soil layers, including clay, sand, and carbon organic contents. These variables were generated using robust ensemble machine learning methods and a large collection of in-situ observations (Hengl 2018). To ensure uniformity in our analysis, these datasets were subsequently resampled to 1 km spatial resolution using the bilinear technique.

Methodology

This section presents the employed methodology for characterizing and assessing vegetation dynamics and their multifaceted drought impacts in the MSEA region during the dry seasons from 2000 to 2022. Here, the multifaceted drought impact implies the consideration of different drought indices, each representing distinct drought types with multi-temporal information. Our analysis delves into the impacts of these indices on vegetation, offering insights on how different drought conditions influence and shape the response of vegetation. In summary, the implemented methodology includes following steps: (1) retrieving and pre-processing satellite and reanalysis time series at monthly resolution; (2) calculating vegetation condition and drought indices; (3) masking non-vegetation and defining the analysis within the dry seasons; (4) analysis of vegetation dynamics and trends, vegetation-drought responses, and drivers. An overview of the workflow is illustrated in Figure 2, and detailed descriptions are presented in subsequent sections.

Selection of vegetation and drought indices

Vegetation condition index (VCI)

NDVI is one of the most widely used indices for monitoring vegetation change and its sensitivity to human and environmental drivers such as land-use change and drought (Fensholt et al. 2009; Z. Li et al. 2013). However, this index presents some limitations. For example, the NDVI primarily measures the greenness of vegetation, and it may not capture subtle changes or water stress (e.g. drought) in vegetation (Goward et al. 1991). If the time-series NDVI data are linearly transformed into the VCI, this VCI data could overcome such challenges (Kogan 1990). For example, the VCI can capture subtle changes while exhibiting strong sensitivity to short- and long-term variations in vegetation. In addition, the VCI measures not only the greenness of vegetation but also its overall health, considering various stressors caused by environmental factors (Kogan 1990; Liu and Kogan 1996). Last but not least, the VCI is expressed as a percentage ranging from 0% (extremely poor vegetation) to 100% (healthy vegetation), making it more interpretable. For this purpose, the time-series VCI measurements are expressed in the following equation (Kogan 1990) (Eq. 1). In this study, the VCI values are calculated per pixel.

$$VCI_i = \left(\frac{NDVI_i - NDVI_{min}}{NDVI_{max} - NDVI_{min}}\right) * 100\% \qquad (1)$$

Where VCI_i is vegetation condition of the i month. The $NDVI_{min}$ and $NDVI_{max}$ are the minimum and maximum NDVI values observed in a specific month during the selected study period (2000–2022), while $NDVI_i$ presents the monthly NDVI values. Although the VCI values can be classified into various levels of vegetation health severity, poor and healthy vegetation are generally considered below and above 50%, respectively (Ha, Uereyen, and Kuenzer 2023; Kogan 1995). Henceforth, the term VCI in this study is also referred to as vegetation condition.

Drought indices

Drought is a complex and multifaceted phenomenon that devastates agriculture and natural terrestrial ecosystems (Ha et al. 2022; Venkatappa et al. 2021). Numerous drought indices have been developed to capture various drought characteristics over the past decades. In this study, however, we selected four key drought indices: SPI, SPEI, SWDI, and TCI because these indices have been widely established in climatology studies (A. K. Mishra and Singh 2010; Seiler, Kogan, and Sullivan 1998) and demonstrated their applicability across diverse geographical regions with different climatic conditions. Each of these indices captures different temporal dimensions and types of drought and its influence on vegetation. For instance, the SPI and SPEI capture multi-temporal

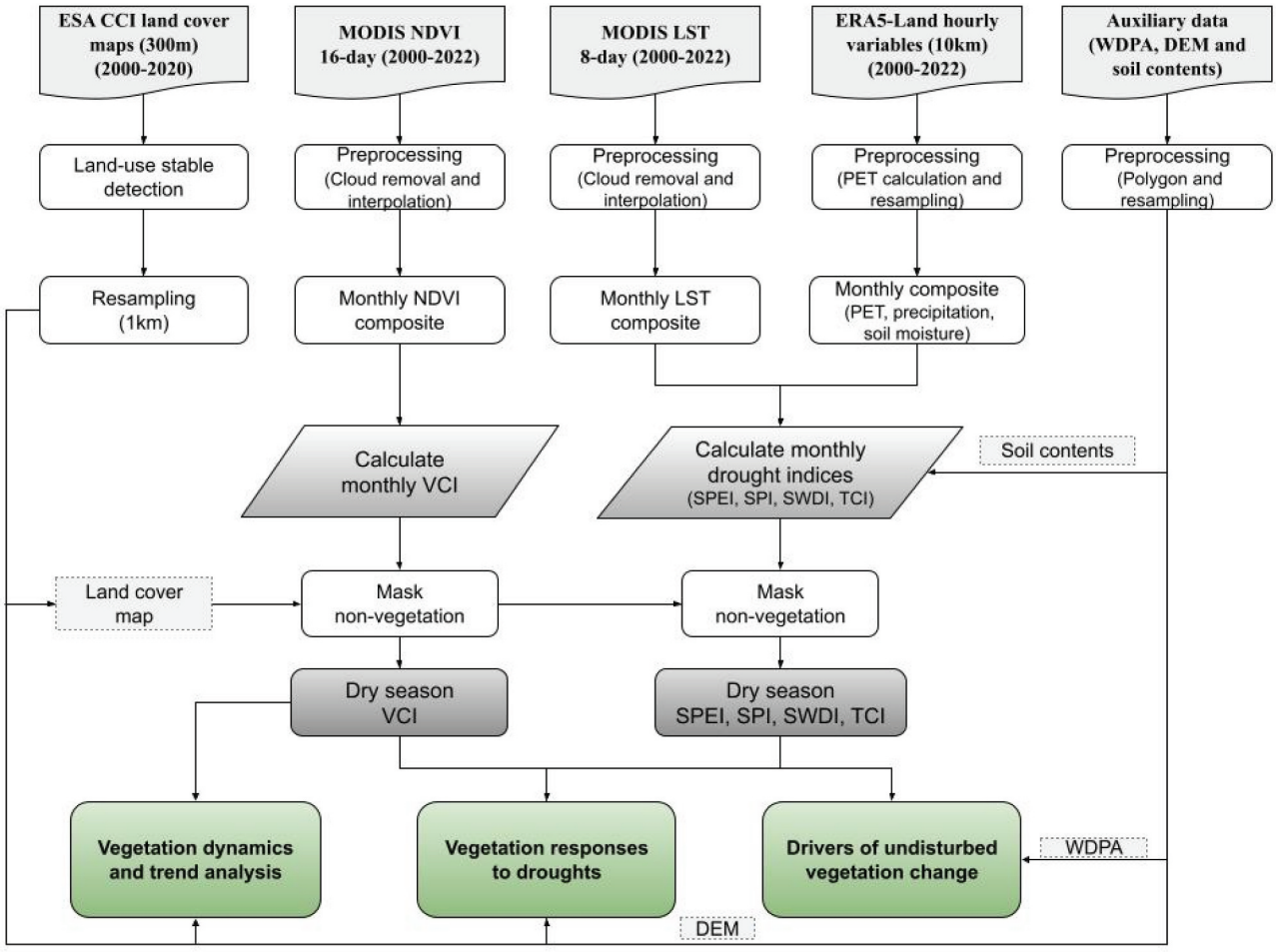

Figure 2. A descriptive workflow showing the analysis of vegetation dynamics and responses to different drought indices as well as the evaluation of drivers of natural and undisturbed vegetation variability during the dry months (November – April) from 2000 to 2022 in the MSEA region. The used drought indices included SPEI (standardized precipitation evapotranspiration index), SPI (standardized precipitation index), TCI (temperature condition index), and SWDI (soil water deficit index), while soil contents referred to clay, sand, and organic carbon layers to retrieve the SWDI. WDPA indicates the World Database on Protected Areas while VCI and DEM means vegetation condition index and digital elevation model, respectively. The SPEI and SPI were calculated over multiple temporal scales of 1, 3, 6, 9, and 12 months.

drought information (McKee, Doesken, and Kleist 1993; Vicente-Serrano, Beguería, and López-Moreno 2010), reflecting different drought types such as meteorological and hydrological droughts, while the SWDI and TCI capture short-term agricultural drought related to soil moisture (A. Mishra et al. 2017) and thermal temperature (Kogan 1995), respectively.

The SPI, a widely used drought index, was initially proposed by McKee, Doesken, and Kleist (1993). This index can be calculated at multi-temporal resolution and derived exclusively from historical precipitation time-series data by fitting a statistical distribution. Here, we selected specific timescales for calculating the SPI to manifest various drought conditions from 2000 to 2022. Specifically, the SPI-1 (1-month) and SPI-3 (3-month) have been widely used to capture short-term drought, while the SPI-6 (6-month) and SPI-9 (9-month) represent medium-term drought, and SPI-12 (12-month) captures longer-term drought conditions (Fang et al. 2019; Ji and Peters 2003). The SPI calculation involves fitting a gamma distribution to the observed precipitation within each month for a selected accumulative timescale (e.g. 1-month, 3-month, and 6-month), and then the resulting values are transformed into a standard normal distribution (Fang et al. 2019; McKee, Doesken, and Kleist 1993). The SPI values typically range from -3 to $+3$, with larger negative (positive) values indicating drier (wetter) conditions. Due to its simplicity and multi-timescale characteristics, the SPI was suggested by

the World Meteorological Organization (WMO) for monitoring and assessing drought (Ha et al. 2022; A. K. Mishra and Singh 2010; WMO 1975).

One of the significant challenges associated with the SPI lies in its exclusive reliance on precipitation data. To address this limitation, a modified version of the SPI, known as SPEI, was developed by Vicente-Serrano, Beguería, and López-Moreno (2010). The SPEI offers a more holistic approach to assessing drought conditions by considering not only precipitation but also evapotranspiration. Here, we calculated the SPEI using the same procedure and timescales as observed in the SPI, but the climatic water balance (D) and log-logistic distribution are used instead. The climatic water balance (D) is derived from the difference between precipitation (P) and PET using the equation Eq. 2 (Vicente-Serrano, Beguería, and López-Moreno 2010).

$$D_i = P_i - PET_i \tag{2}$$

Where D_i indicates monthly water balance, and P_i and PET_i denotes the precipitation and PET at month i, respectively.

In tropical regions, vegetation exhibits high sensitivity to temperature variations. Extreme high or cold temperatures can induce negative adversity to vegetation vigor. Hence, we calculated the TCI, which reflects different responses of vegetation to thermal stress. The TCI is derived from MODIS-based LST by relative calculations using the minimum and maximum temperatures recorded during the specified period (Kogan 1995), expressed in Eq. 3.

$$TCI_i = \left(\frac{T_{max} - T_i}{T_{max} - T_{min}}\right) * 100\% \tag{3}$$

Where TCI_i is temperature condition index of the i month. The T_{min} and T_{max} are the minimum and maximum temperature values observed in a specific month during the selected study period (2000–2022), while T_i presents the monthly temperatures. Higher TCI values indicate wetter conditions, whereas lower values denote drier conditions, and normal conditions are around 50% (Kogan 1995).

While the SPI, SPEI, and TCI provides critical information on meteorological and hydrological aspects of drought, they may not directly capture the soil moisture. By contrast, the SWDI offers robust insights into soil moisture conditions. Notably, this indicator is capable of detecting soil moisture deficits even before they become evident in precipitation data, making it a useful tool for monitoring agricultural drought (A. Mishra et al. 2017). Here, we calculated the SWDI using relevant soil properties and monthly topsoil moisture (7-28 cm depths), as established in previous studies (Martínez-Fernández et al. 2015; A. Mishra et al. 2017). Lower negative SWDI values imply drier conditions, while more positive values signify wetter conditions, with values approaching zero indicating non-drought conditions.

Analysis of vegetation dynamics and their drought impacts

Trends of vegetation time series

Monitoring vegetation dynamics and trends provide crucial insights into the ecological health of our planet and enable the assessment of the impacts of climate change as well as land-use and ecosystem disturbances. In this study, we combined the Modified Mann-Kendall (MMK) test and the Sen's slope method to detect interannual trends in vegetation vigor during the dry growing seasons spanning from 2000 to 2022 across the MSEA region. These methods are non-parametric and robust, capable of handling outliers, missing values, and non-normally distributed data measurements (Z. Li et al. 2013). The MMK test determines the trend direction, whereas the Sen's slope measures the magnitude of the slope (Frazier et al. 2018). A positive slope denotes an increasing trend in vegetation, while a negative slope signifies a decrease.

The Mann-Kendall (MK) significance test, proposed by Kendall and Henry Mann (Kendall 1948; Mann 1945), has been commonly used for estimating temporal trends in vegetation and climatology studies (De Jong et al. 2011; Guo et al. 2018). However, this method can yield lower sample variance measures due to its sensitivity to autocorrelated time series data (Guo et al. 2018), as is often observed in vegetation and climate time series. To address this issue, Hamed and Rao (1998) introduced the MMK test, and this method became more robust in the presence of temporal serial correlation data. In addition, vegetation time-series observations may be influenced by various factors, such as human activities and sensor-related issues. Thus, this study determined the overall trend by calculating the statistically significant trend for a specific period (e.g. 10 years) and averaged

across different time intervals while also accounting for local trend. Specifically, a statistically significant trend was calculated for each period extending over a decade (e.g. 2000–2010, 2001–2011, 2002–2012, and so on). The overall trend over the study period was subsequently averaged over all intervals (12 intervals). A significant trend in the MMK test is subsequently identified at a level of p-value ≤0.05 per pixel basis, whereas non-significant trend values are discarded from the analysis.

Spatial patterns of vegetation response to drought

This study employed Spearman's rank correlation analysis to investigate the responses of vegetation condition to different drought indices during the dry growing seasons from 2000 to 2022. The Spearman method is a non-parametric measure of the strength and direction of the monotonic relationship between the two variables (Bisquert et al. 2017; Tran et al. 2023). This technique is recognized as more robust to non-linear relationships and non-normally distributed data, which are frequently encountered in vegetation and climate time series (Cao et al. 2022). Time series of vegetation condition and drought indices were initially transformed into anomalies to address potential spurious correlation (Udelhoven et al. 2009). Subsequently, we identified the maximum correlation coefficients (MCC) between vegetation condition and SPEI and SPI across multiple timescales (e.g. 1, 3, 6, 9, 12 months), while calculating the correlation values for TCI and SWDI at each pixel. Different vegetation types may exhibit different sensitivities to drought durations, and the MCC highlighted the most robust response of vegetation to the SPEI and SPI. The Spearman correlation coefficients range from -1 to 1, where values closer to ± 1 (0) indicate stronger (weaker) monotonic relationships, respectively. Positive correlations suggest that vegetation tends to deteriorate as drought severity increases, while negative correlations indicate an inverse association. The coefficients calculated at each pixel are identified at $p \leq 0.05$ significance level.

Driver analysis of natural and undisturbed vegetation

Global warming poses a significant threat to the functioning of terrestrial vegetation and ecosystems (Forzieri et al. 2022; McDowell and Allen 2015). Therefore, it is imperative to understand how drought conditions drive natural and undisturbed vegetation, as this serves as a critical reference point. In this study, we selected natural vegetation areas (e.g. undisturbed forests and shrubs) where human activities are either absent or negligible. Hence, our analysis was confined to protected areas, allowing us to elucidate the driving factors of change in natural and undisturbed vegetation across the MSEA region during the dry growing seasons between 2000 and 2022. While precipitation, temperature, and soil moisture are widely used and recognized as the most direct indicators for identifying contributions to vegetation variability, they come with major limitations related to drought characteristics. For instance, raw precipitation fails to capture both short-term and long-term droughts/impacts and lacks multi-temporal information (Lloyd-Hughes and Saunders 2002). By contrast, drought indices provide a more holistic, time-sensitive, and spatially consistent assessment of drought conditions (Lloyd-Hughes and Saunders 2002; A. K. Mishra and Singh 2010). The SPEI, for example, can provide drought information across different timescales, representing various drought types. In addition, the SPEI takes the temperature and precipitation into account, so it offers more relevant insights into the water availability within ecosystems. Here, our analysis considered several land-atmosphere-based drought indices as the drivers of vegetation dynamics, including SPI-1, SPI-3, SPI-6, SPI-9, SPI-12, SPEI-1, SPEI-3, SPEI-6, SPEI-9, SPEI-12, TCI, and SWDI.

To determine the relative importance of driving factors on vegetation dynamics, we performed the random forest (RF) regression (Breiman 2001) and applied the SHapley Additive exPlanations (SHAP) method (Lundberg and Lee 2017). The RF regression, a non-parametric ensemble learning method, offers robustness against outliers, non-linearity, overfitting, and autocorrelation in time-series data (Breiman 2001; Gessner et al. 2015). It constructs a large number of decision trees by repeatedly selecting random subsets of the original datasets with replacement, a process known as bootstrapping (Breiman 2001). In our study, we trained the RF regression using time-series drought indices to predict the vegetation condition (VCI) with 500 decision trees. While the RF regression model can measure the overall importance of features, it lacks the capacity to deliver individual insights for each specific prediction and fails to explain why and how these features influence

vegetation conditions (Lange et al. 2022). Thus, the RF regression was combined with the SHAP method to explain the overall and detailed impacts of different drought conditions on vegetation change. The SHAP technique computes the Shapley values from a trained machine learning model (e.g. RF regression), providing the directional contributions and strength of each observation to the model output (Lundberg and Lee 2017). Positive (negative) SHAP values suggest a positive (negative) impact on the prediction of the response variable, respectively. The overall relative importance of each feature is subsequently determined by calculating the mean of the absolute SHAP values across all individual observations. In this study, the SHAP method and RF regression are performed using Python SHAP and scikit-learn packages, respectively.

Results and discussion

Dynamics and trends of vegetation condition

Spatiotemporal vegetation patterns

In the MSEA region, the vegetation condition exhibited diverse spatial and temporal patterns across various land cover types and countries during the dry seasons from 2000 to 2022. Overall, larger areas of stressed vegetation (VCI ≤50) were detected in Thailand, Cambodia, and Myanmar in certain years. Notably, rainfed croplands and evergreen forests generally suffered from poorer vegetation health.

As can be seen in Figure 3, vegetation condition experienced noticeable stress in 2004, 2005, 2007, 2010, and 2020. Almost 60% of the dry seasons in the region recorded large-area vegetation disturbances (with over 40% of affected areas each year) over the study period. For example, nearly 80% of the vegetation in the MSEA region witnessed signs of degradation in 2005, while in 2010, this proportion peaked at almost 75%. In recent years, there have been distinct variations in stressed and productive vegetation. The highest rates of healthy vegetation were recorded in 2018 and 2022 (~85%) across the region. In contrast, large areas of stressed vegetation were evident in 2019, 2020, and 2021 (Figure 3). These findings were aligned with recent studies (Ha, Uereyen, and Kuenzer 2023; B. Zhang et al. 2014). Widespread instances of vegetation stress were primarily associated with drought hazards. A recent analysis of ground-based drought data revealed that the MSEA region suffered from multiple severe drought episodes in 2005, 2010, 2015, 2019, and 2020 (Ha et al. 2022). These years coincided with large areas of stressed vegetation in the region (Figure 3). Also, B. Zhang et al. (2014) examined vegetation productivity in the same region during the drought years and revealed that the severe drought event in 2005 reduced nearly 15% of vegetation productivity.

Given the spatiotemporal dynamics of vegetation types and management practices in each MSEA country, areas of stressed vegetation were temporally varied over the study period. Figure 4 shows the temporal evolution of stressed vegetation areas across different land cover types across the MSEA countries. Overall, Cambodia had the most significant areas of stressed vegetation over the study period, while Vietnam suffered from the least vegetation deterioration, especially over the past ten years. Most areas of stressed vegetation were found in rainfed cropland and forests. For example, nearly 30% of rainfed cropland in Cambodia suffered from stress in 2005, and this figure remained relatively similar over the study period. In Thailand, this proportion peaked in 2005 (~25%) and 2020 (17%), while Laos and Myanmar generally had less than 10% of stressed rainfed croplands.

In comparison, Vietnam had below 5% of stressed rainfed cropland in most observed years (Figure 4). Notably, Vietnam together with Laos and Myanmar had much smaller proportions of stressed rainfed cropland areas than that in Cambodia and Thailand. Venkatappa et al. (2021) assessed the impact of drought on rainfed cropland in Southeast Asian countries and reported that Cambodia and Thailand had the highest proportion of damaged rainfed cropland, about 40% and 30%, respectively. By contrast, Vietnam witnessed less than 10% of its rainfed cropland affected during the same period. These discrepancies could be attributable to several factors such as climatic factors, resource availability, and cropping practices. For example, Vietnam had a relatively higher precipitation rate and lower temperatures than Thailand and Cambodia during the dry seasons (Hersbach et al. 2020). In Myanmar, Cornish et al. (2018) reported that short-duration crops and shifting sowing dates were commonly practiced in drought-prone areas to minimize the risks in rainfed cropping systems (Radanielson et al. 2019).

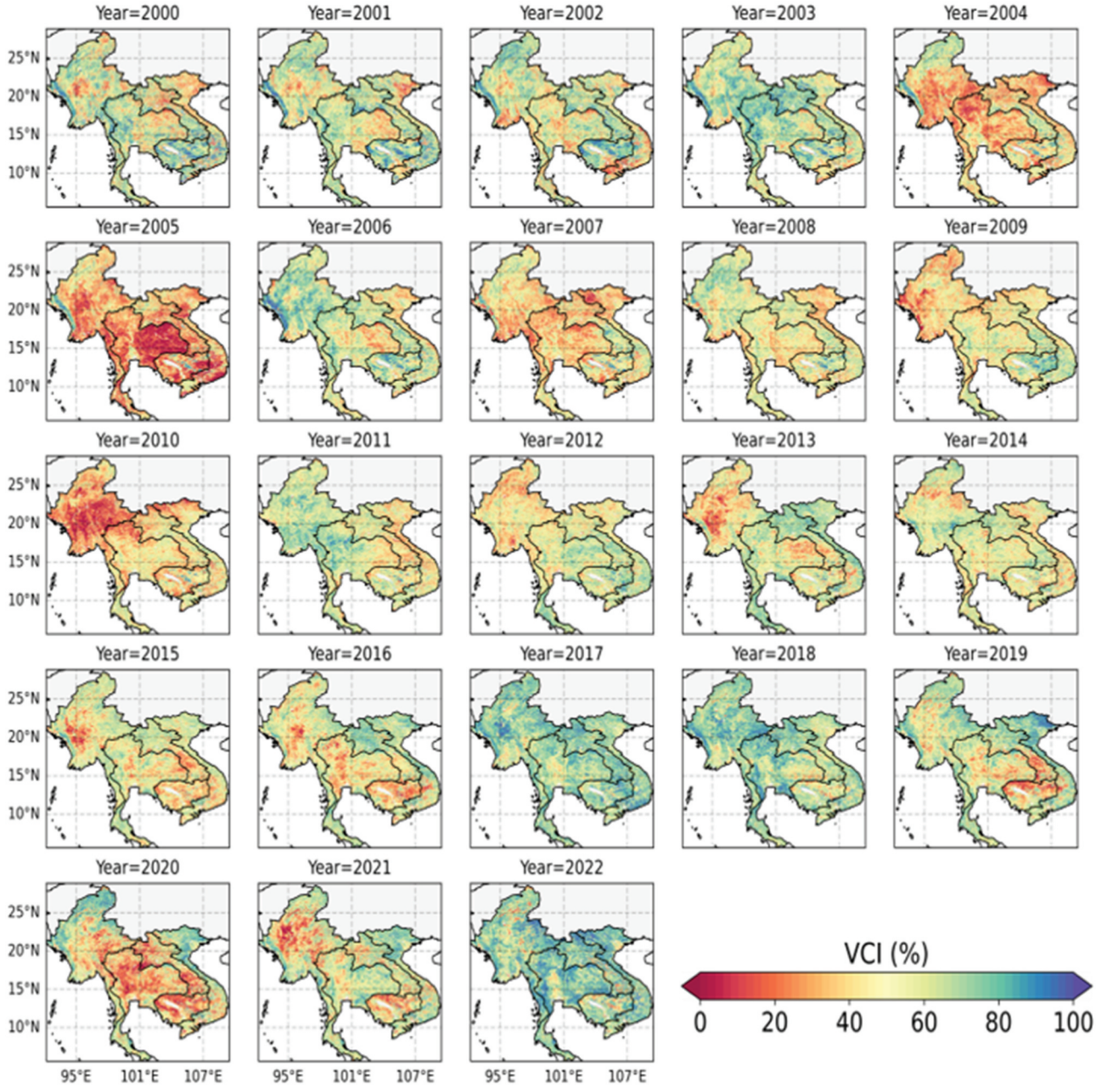

Figure 3. Spatial variability of vegetation condition over the MSEA region during the dry growing seasons from 2000 to 2022. The blue represents healthier vegetation, whereas reddish color implies poorer vegetation condition.

Among the remaining vegetation types, evergreen and mixed forests experienced larger areas of disturbances than shrubland and deciduous forests over the years, especially during the drought years. Cambodia had the largest area of forest disturbance, being above 10% in 2005, 2010, and 2020, while Laos and Myanmar ranked second, with 5 to 10% of the forests being stressed (Figure 4). Vietnam and Thailand experienced below 5% stressed forests (e.g. evergreen forests). Irrigated cropland and deciduous forests had little sign of degradation. Specifically, only less than 3% of the respective areas were under stress in most observed years. Higher proportions of stressed forests in Cambodia, Laos, and Myanmar were in accordance with recent studies (Chen et al. 2023; Grogan et al. 2015; Hansen et al. 2013), primarily due to drought and deforestation.

Vegetation trend analysis

Despite several years of vegetation stress, vegetation across the MSEA region had generally shown a greening trend over the past two decades. Figure 5

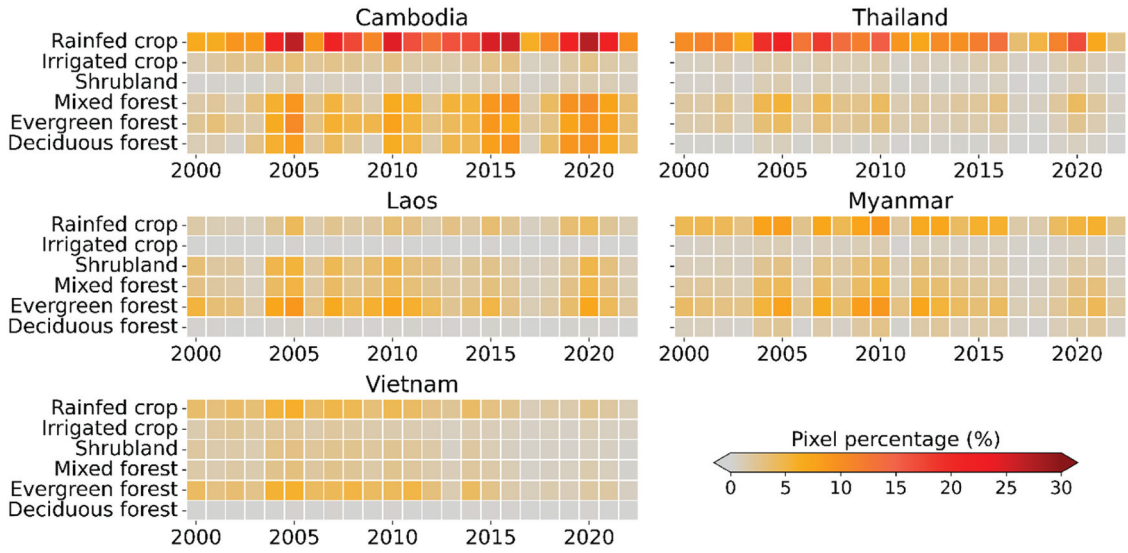

Figure 4. Temporal variations in the percentage of stressed vegetation areas across six land cover types in the MSEA countries during the dry seasons from 2000 to 2022. Stressed vegetation corresponds to areas where the VCI ≤ 50, indicating drought-induced vegetation condition.

displays the spatial pattern of statistically significant vegetation greening trend (p-value ≤0.05) detected during the dry seasons from 2000 to 2022. It is observed that nearly 70% of the MSEA region experienced an increasing vegetation trend, and this greening was predominantly in the northern region (Figure 5a). Our detected spatial trend was also clearly observed in recent studies. For example, Ha, Uereyen, and Kuenzer (2023) employed time series MODIS-based vegetation and indicated that greening and browning vegetation were dominated in the northern Vietnam and Cambodia, respectively. In more details, Vietnam had the highest proportion of pixels exhibiting a greening trend (~75%), followed by Thailand (~70%). Myanmar and Laos also saw substantial greening, with proportions of 70% and 62%, respectively. In contrast, Cambodia had the lowest percentage of greening pixels, with only around 40%. Notably, there was a distinct pattern of vegetation trends between Thailand and its neighboring countries. For instance, within 50 km of the Thai-Cambodia border, Thailand exhibited a significant rise in vegetation greening, averaging 2.1% per year (in VCI units) during the dry seasons from 2000 to 2022 (Figure 5a). Cambodia, however, witnessed a significant decline in vegetation at a rate of – 2% per year during the same period. This distinctive pattern can be attributed to the stringent protection and control measures imposed on forests in Thailand. Southworth, Nagendra, and Cassidy (2012) revealed that the Thai military plays a crucial role in safeguarding these forests, bolstered by the presence of protected areas

Apart from spatial distribution of the vegetation trend, the line plots from Figure 5 depict the temporal variations of overall vegetation trend across the MSEA countries. Again, Vietnam exhibited a consistent trend in greening vegetation over the past 22 years. Conversely, Cambodia showed an overall decline in the vegetation trend (Figure 5b). Despite some temporal variations, vegetation condition in Myanmar, Laos, and Thailand remained relatively stable (non-significant trend) in most land cover types (Figure 6). Notably, a significant decline in vegetation was found in Cambodia across different land cover types, with the most substantial reduction occurring in deciduous forests and shrubs at a rate of – 1% per year (Figure 6). By contrast, Vietnam witnessed a significant greening trend, averaging above 1% per year in most land cover types (Figure 6). It can be observed that a large area of Myanmar and southern Laos indicated a sign of significant browning vegetation (Figure 5a), but examining individual vegetation types showed a statistically non-significant trend in most cases (Figure 6). Country-specific disturbances and data aggregation could be responsible for these variations. For example, the per-pixel trend analysis used in this study enables detecting location-specific and subtle changes in vegetation, while aggregating data

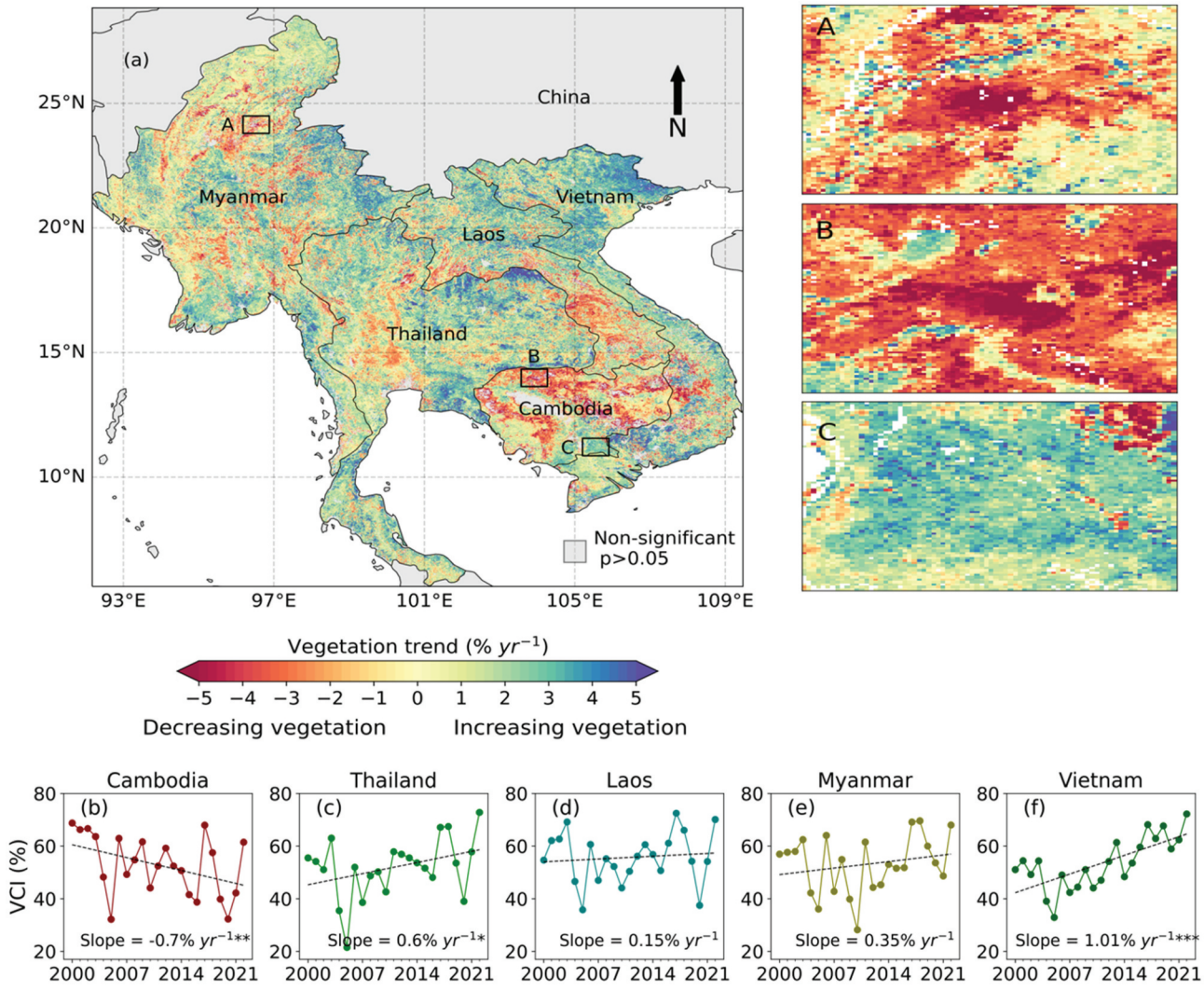

Figure 5. Spatial variability of vegetation condition trend (a) over the dry growing seasons from 2000 to 2022. Red colors represent negative vegetation trend (decreasing vegetation) and blue implies positive trend (increasing vegetation). Right-side subplots (A-C) shows the trend of vegetation condition in three exemplified locations with different land cover characteristics. Subplots (A-B) represent vegetation trends where forest was cut down or disturbed whereas the subplot (C) displays the trend of vegetation in the Lower Mekong Delta, where agriculture is dominant and stayed stable over the study period. The line plots represent the overall trend of vegetation across the MSEA countries (b) Cambodia, (c) Thailand, (d) Laos, (e) Myanmar, and (f) Vietnam. Statistically significant slope values in the line plots are marked with three asterisks (***, p-value ≤0.01), two asterisks (**, p-value ≤0.05), and one asterisk (*, p-value ≤0.1).

across land cover types over large areas may struggle to capture more local and transient variability. It is also important to note that land-use types in the MSEA countries are significantly fragmented and intertwined. For instance, Kuenzer et al. (2018) examined the consistency among six global land cover products (e.g. MODIS land cover, GlobCover) in the MSEA region, and their findings indicated large disparities among these products. This means that the temporal trend of vegetation across land cover types in the MSEA countries could be largely influenced by the land cover product.

While several factors may contribute to spatiotemporal variations in the vegetation trends across the study region, drought and forest disturbances are likely the major drivers. For example, Cambodia ranked among the countries with the highest rate of forest loss worldwide (Hansen et al. 2013), with nearly 50 thousand km^2 of forest loss from 1998 to 2018 (Namkhan et al. 2021). Likewise, Myanmar also lost approximately 30 thousand km^2 of its forests over the same period (Namkhan et al. 2021). Our trend analysis indicated that nearly 70% of Cambodian forests suffered from a declining trend over the past 22 years,

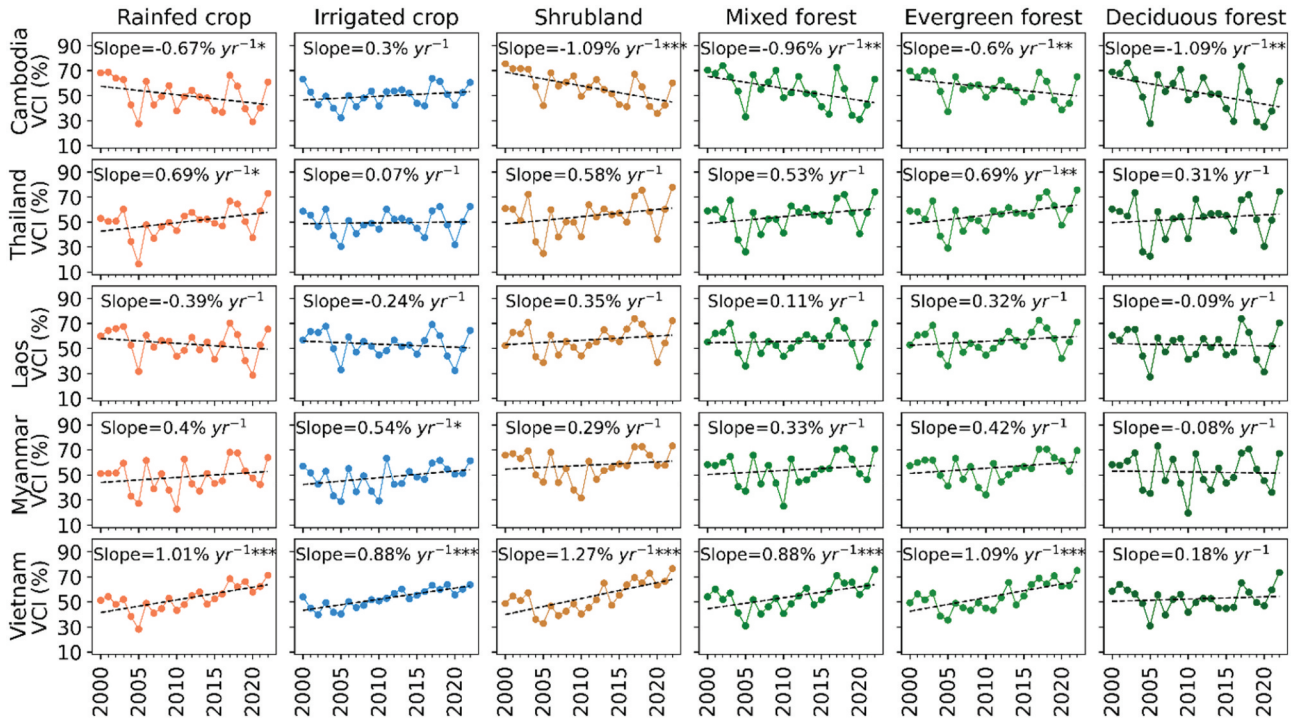

Figure 6. Temporal trends of vegetation condition during the dry growing seasons across different landcover types in the MSEA countries. The vertical columns represent six land cover types and horizontal rows represent five different countries (e.g. Cambodia, Thailand, Laos, Myanmar, and Vietnam). Statistically significant slope values are marked with three asterisks (***, p-value ≤0.01), two asterisks (**, p-value ≤0.05), and (*, p-value ≤0.1).

while this figure for Myanmar was 32%. As an example, a negative trend in forested areas are displayed in the subplots (A) and (B) of Figure 5. In Vietnam, large areas of greening vegetation were detected in the north, and this was primarily due to forest plantation initiatives and intensive agricultural practices (Nambiar 2021).

Noticeably, the Central Highlands of Vietnam showed a significant decline in vegetation, possibly driven by the expansion of industrial crops (e.g. coffee plantations) into forested areas (Zeng et al. 2018). Also, this area was affected by the worst drought in 2016 (Le et al. 2020). In Laos, browning trends were identified in large proportions of the southern provinces, being consistent with recent findings of widespread forest loss (Cui et al. 2023) originating from shifting agriculture activities (Chen et al. 2023). This shift has resulted in the expansion of rainfed cropland areas, and recent droughts significantly exacerbated the declining trends. In comparison, most of the Lower Mekong Delta experienced greening trends over the past 22 years. This greening trend was clearly visible in Figure 5 (subplot C), where irrigated rice-growing systems were dominant (Ha, Uereyen, and Kuenzer 2023).

Apart from drought and forest disturbances, elevation and land-use patterns may also influence the trend of vegetation. Figure 7 shows the distribution of significant vegetation trend values (p-value ≤0.05) under various elevation bins and land cover characteristics across the MSEA region. Clearly, higher vegetation trends were primarily found at higher elevation zones across the land cover types (Figure 7). Specifically, vegetation condition at altitudes above 1000 m exhibited the highest positive trend while the elevation bins within the 100-500 m exhibited lower trends. For example, a gradual increase in the vegetation trend from low to higher elevations was identified for evergreen forest, with nearly 2% (in VCI unit) above 1000 m. Notably, deciduous forest witnessed the largest increase in vegetation trend, starting from – 2% (in VCI unit) at 100 m to nearly 2% above 1000 m (Figure 7). Rainfed and irrigated cropland displayed a relative stable trend across the elevation bins while shrubland and mixed forest showed a slight increase in the vegetation trend at higher elevation areas. Multiple factors can contribute to varying vegetation

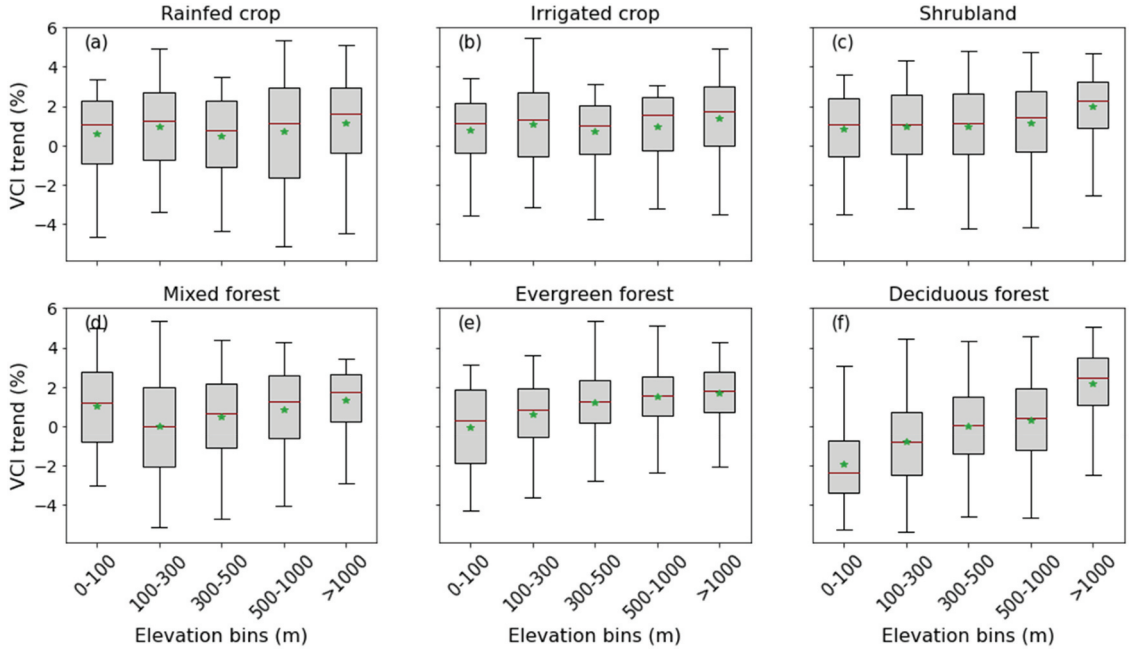

Figure 7. Boxplots of spatially averaged vegetation trend values (p-value ≤ 0.05) in the MSEA region under different elevations and land cover types during the dry seasons from 2000 to 2022. The green asterisk and red line in each box represent mean and median values, respectively.

trends across elevations. Higher precipitation and cooler temperature in higher altitudes can facilitate the vegetation growth compared to low elevation zones (Daly et al. 2008; You et al. 2013). Also, soil quality and water retention capabilities are likely better at higher elevations due to lower rates of soil erosion and less intensive land use. The presence of rich organic matter (e.g. leaf and plant debris) in these regions enhances water retention, providing a stable supply of moisture for vegetation even during the dry periods (Cislaghi et al. 2019). In addition, these areas were generally forests and less impacted by human activities (e.g. agricultural shifting and land use conversion), resulting in less deforestation and land degradation (Zhenzhong et al. 2021). Among the examined land cover types, deciduous forests, on average, experienced a negative trend, particularly in lower elevation zones, while other land cover types witnessed a positive trajectory. In case of deciduous forests, it is observed that nearly 85% of this forest is located in Cambodia under 100 m above the seas and witnessed negative trends. By contrast, deciduous forests in high elevations (above 500 m) are primarily observed in Myanmar (~73%) and Thailand (~17%), where positive trends were more dominant. These patterns were consistent with the spatial distribution of the VCI trend demonstrated in Figure 5. Cambodian forests witnessed large decline primarily due to drought and forest disturbance (e.g. deforestation) over the past 20 years (Hansen et al. 2013; Ha, Uereyen, and Kuenzer 2023). This observation was also reported in other studies (Jeganathan, Dash, and Atkinson 2014; Zoungrana et al. 2018), indicating that tropical deciduous forests in the MSEA are more vulnerable at lower elevation areas.

Responses of vegetation to droughts

Spatial patterns of vegetation-drought responses

To study vegetation condition response to varying drought conditions across the MSEA region, we calculated Spearman per-pixel correlations between vegetation and multiple drought indices (SPEI, SPI, SWDI, and TCI) at different time scales during the dry seasons from 2000 to 2022. Overall, there was a significant positive correlation between vegetation condition (VCI) and drought indices (Figure 8). Notably, the TCI generally had a higher relationship with vegetation condition among the examined drought indices, with the central region of Vietnam exhibiting non-significant correlations in most cases. Our per-pixel analysis found that the proportion of statistically significant coefficients varied from 56 to 66% between vegetation and drought indices across

the MSEA region. The SPEI and SPI had the largest proportion of significant coefficients, with nearly 66%, while the SWDI witnessed only 56%.

Figure 8(a,b) displays a consistent positive relationship between vegetation and the drought indices SPEI and SPI across the MSEA region. Vegetation in the MSEA region had a higher response to short-timescale SPEI and SPI, and this pattern was more evident in Central Myanmar and northern Thailand. For example, nearly 90% of the MSEA region showed the largest response of vegetation to SPEI-1, SPEI-3, and SPEI-6 (subplot in Figure 8a). In addition, nearly 56% of the MSEA region was characterized by a significant positive correlation between vegetation and SWDI (Figure 8c), resulting in an average R-value of about 0.6. Likewise, nearly 60% of the study area depicted statistically significant positive correlations between vegetation health and TCI (Figure 8d) over the study period. In comparison, only 3% of the area showed such negative correlations between the two datasets, and the rest indicated statistically non-significant correlations. Notably, Cambodia had the most substantial area with positive correlations between the TCI and vegetation (~82%), followed by Thailand (~72%), and Myanmar (~60%). Despite spatial variations, the average R coefficients in these countries ranged from 0.35 to 0.82 (Figure 8d). By contrast, Vietnam showed the modest R coefficients, averaging around 0.35, covering around 35% of the country. Most of Vietnamese central and northern

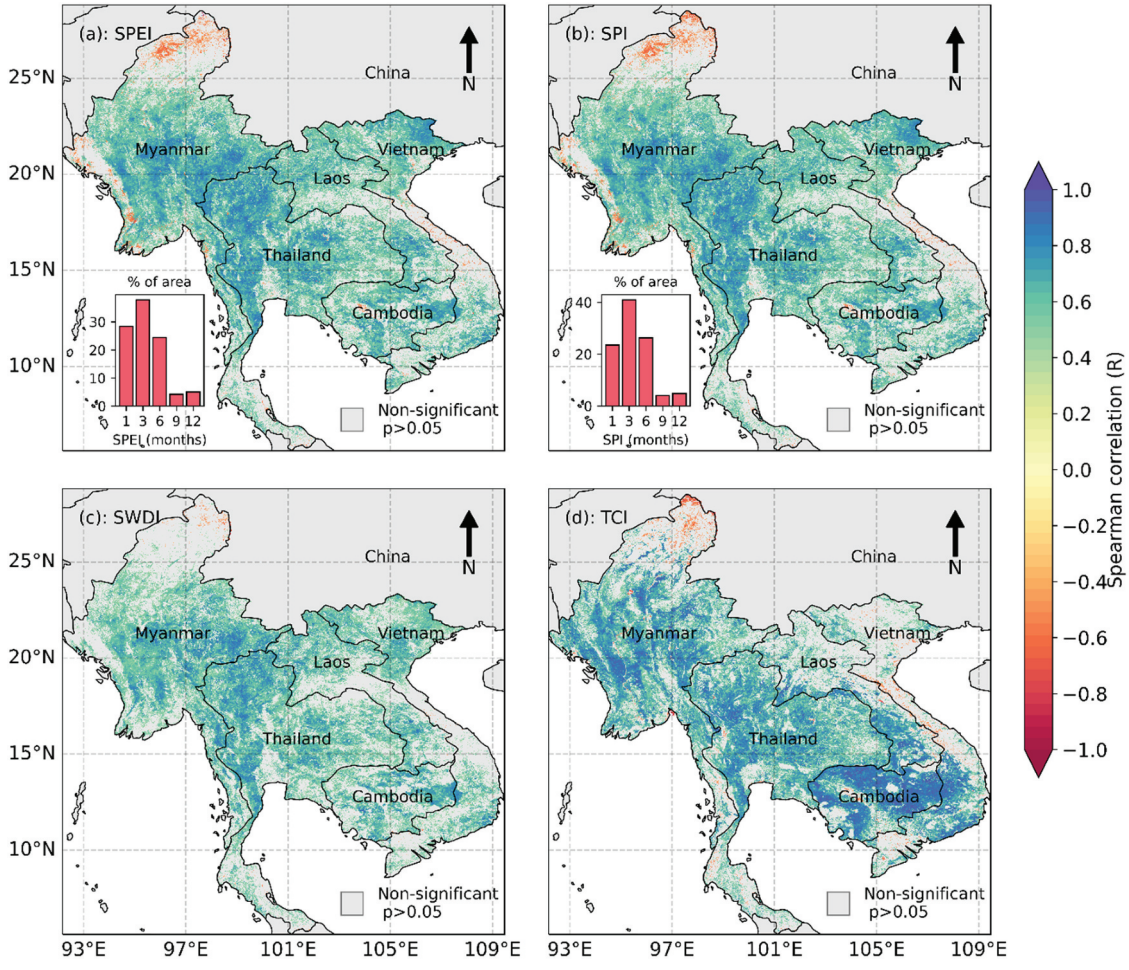

Figure 8. Spatial patterns of Spearman coefficients between vegetation conditions and drought indices (a: SPEI, b: SPI, c: SWDI, and d: TCI) during the dry seasons between 2000 and 2022. Red (blue) colors represent the negative (positive) values of correlation coefficients (p-value ≤0.05) between vegetation and drought conditions. The gray areas indicate statistically non-significant pixels and masked areas. The inset bar plots in (a-b) indicate the proportion of the total area having the largest coefficients at the selected timescales. The SPEI and SPI represents the maximum correlation coefficient with vegetation condition at the five drought timescales (1-month, 3-month, 6-month, 9-month, and 12-month). SPEI: standardized precipitation evapotranspiration index, SPI: standardized precipitation index, SWDI: soil water deficit index, and TCI: temperature condition index.

regions witnessed non-significant correlations, while the southern regions showed relatively high vegetation-drought responses, particularly along the Central Highlands, extending toward the southern coast of Vietnam (Figure 8d).

This relationship suggests that vegetation condition tends to thrive as values of drought indices increase, indicating wetter conditions. In other words, vegetation in the MSEA region is sensitive to changes in soil moisture and water availability, making it more susceptible to drought. These positive correlations between vegetation and drought indices agreed with previous studies (Ji and Peters 2003; A. Zhao et al. 2018), and that vegetation generally responds to shorter drought indices (e.g. SPEI-1, SPEI-3) in tropical areas (Vicente-Serrano et al. 2013). It is noteworthy, however, that a large portion of the central Vietnam and upper Myanmar typically experienced statistically non-significant relationships between vegetation and drought indices. This absence can be attributed to a range of localized factors. In mountain ranges, microclimatic variations driven by altitude and topography create diverse weather patterns that can independently influence vegetation health. For example, in Myanmar's northern mountains, presence of fog and dew can provide moisture that supports vegetation even during periods of low precipitation, thereby possibly weakening the correlation with the drought indices. Likewise, coastal areas in Vietnam experience sea breezes and high humidity levels that can sustain vegetation despite drought conditions, masking the expected correlation. One common observation in these regions is an abundance of precipitation, which can stabilize vegetation growth. Moreover, human activities such as agricultural practices and land use changes can artificially bolster vegetation resilience to drought (Fan et al. 2023). These factors underscore the complexity of ecosystem responses to climate variables and highlight the need for localized studies to better assess the interplay between drought indices and vegetation dynamics in these specific regions.

Responses of vegetation to droughts under different elevations and land cover types

Vegetation responses to droughts can be influenced by different factors, including environmental and human-induced elements. In this study, we examined the responses of vegetation to multifaceted drought indices at statistically significant pixels in consideration of different land cover types and elevation characteristics. Overall, vegetation condition exhibited a significantly positive response to drought indices, but its responses varied across land cover types and elevation zones in the MSEA region.

Figure 9 depicts the spatially averaged coefficients (p-value ≤0.05) between vegetation and the drought indices across elevation bins with respect to specific land cover types. It is observed that vegetation condition appears to have a higher response to TCI at lower elevations. For instance, deciduous forests had the strongest response to the TCI at below 100 m elevation zones ($R = 0.85$), while its response at above 1000 m was notably lower ($R = 0.56$). In comparison, higher vegetation responses to the remaining drought indices (SPEI, SPI, SWDI) were found in 300–1000 m elevated areas. In this regard, the highest vegetation-drought response was especially observed at 300–500 m zones (Figure 9) across rainfed crop ($R = [0.63–0.7]$), mixed forest ($R = [0.63–0.69]$), and deciduous forest ($R = [0.62–0.73]$). This pattern suggests that vegetation condition at elevation zones between 300 and 1000 m is more likely vulnerable to drought variability. Also, this finding is consistent with the lower vegetation trend in these areas (Figure 7a). Furthermore, it can be noted that vegetation above 1000 m witnessed a lower response to drought indices (Figure 9). At the same time, it is determined that vegetation trend was highest at these altitudes (Figure 7a). While limited research has explored the relationship between vegetation and multifaceted drought indices across different elevations, Y. Wang et al. (2021) studied the responses of vegetation to droughts (SPEI and SPI) in the Tibetan Plateau and found that higher elevations tended to have lower responses to vegetation productivity.

In terms of vegetation-drought responses across land cover types, deciduous and mixed forests had the highest response to drought indices, being followed by rainfed croplands. For example, the correlation between TCI and deciduous forests, on average, was found to be ~ 0.73. By contrast, other remaining land cover types had much lower responses to drought indices, especially in lower elevations. For example, shrubland was less sensitive to drought

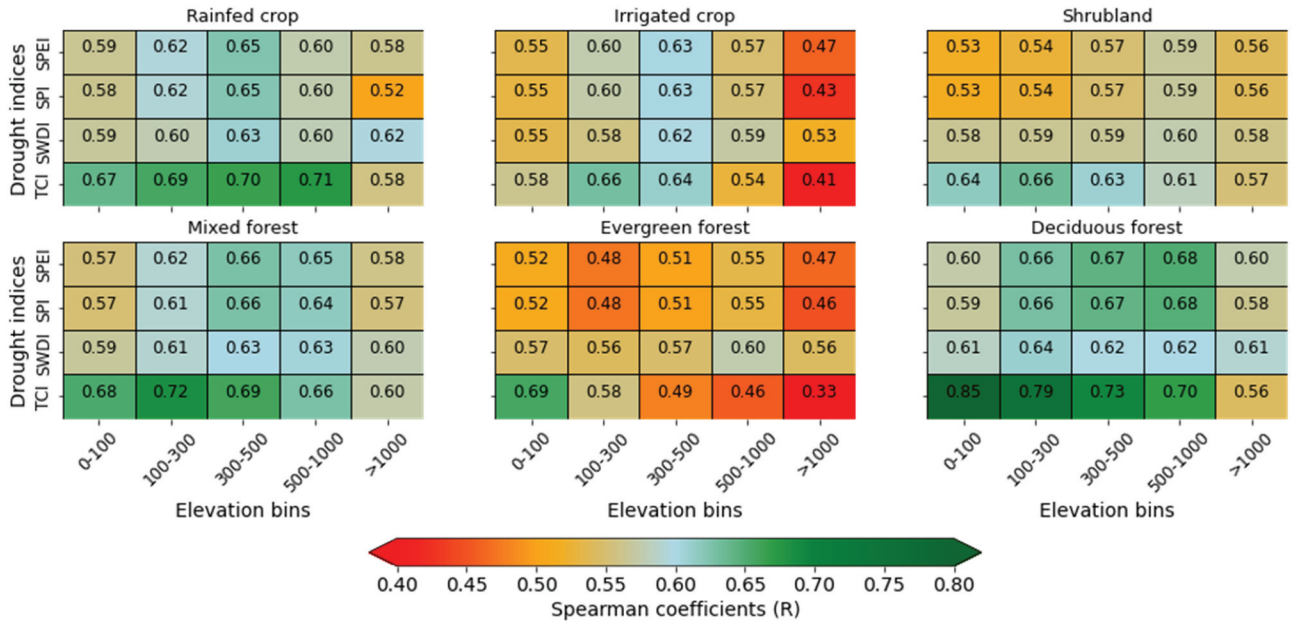

Figure 9. Heatmap shows the distribution of spatially averaged coefficients (p-value ≤0.05). These coefficients highlight the correlation between vegetation condition and four drought indices across the land cover categories during the dry growing seasons between 2000 and 2022. The SPEI and SPI represents the maximum correlation coefficient with vegetation condition from multi-temporal timescales (1-month, 3-month, 6-month, 9-month, and 12-month). SPEI: standardized precipitation evapotranspiration index, SPI: standardized precipitation index, SWDI: soil water deficit index, and TCI: temperature condition index.

indices with a R between 0.53 and 0.64. Notably, evergreen forests had the lowest response to all examined drought indices, suggesting a higher resilience to droughts in the tropical regions. This might be explained through the fact that tropical evergreen forests maintain better light-use efficiency of photosynthesis even during the dry conditions (Huang and Xia 2019). It is also observed that evergreen forests in the MSEA region are primarily found in higher elevations (e.g. northern Myanmar), where climatic conditions experience less extreme events (Feng et al. 2020).

Drivers of natural and undisturbed vegetation dynamics

In this study, the RF model was trained using the entire sample data from 2000 to 2022, and subsequently the SHAP values were derived from this trained model. Although the model optimization is not the primary focus, we assessed the model's performance, finding an R^2 (coefficient of determination) of 0.94 on the entire training dataset over the protected areas. This result indicated that our trained model performed well, suggesting a reasonable level of accuracy for proceeding with the SHAP analysis.

Divergent drought conditions can significantly impact the condition of natural vegetation (Chang et al. 2023), especially in tropical and subtropical regions. In the following, we explored the roles of different drought indices driving natural and undisturbed vegetation variability during the dry seasons across the MSEA region from 2000 to 2022. These indices, each representing distinct aspects of drought conditions, were categorized into short-term (e.g. SPEI-1, SPEI-3, SPI-1, SPI-3, TCI, and SWDI), medium-term (e.g. SPI-6, SPI-9, SPEI-6, and SPIE-9), and long-term drought conditions (e.g. SPEI-12 and SPI-12).

In this regard, Figure 10a shows the relative importance of drought indicators driving natural vegetation dynamics. Generally, this figure indicates that natural and undisturbed vegetation appears to be exceptionally influenced by short-term disturbances. For instance, short-term drought conditions explained nearly 93% of variations in natural vegetation changes in the MSEA region. In particular, the SPEI-3 was the most influential contributor, explaining approximately 35% of the observed changes. This finding underscores the significant impact of precipitation and temperature patterns occurring over three months on natural and undisturbed vegetation. The TCI ranked second, accounting for about 20% of the

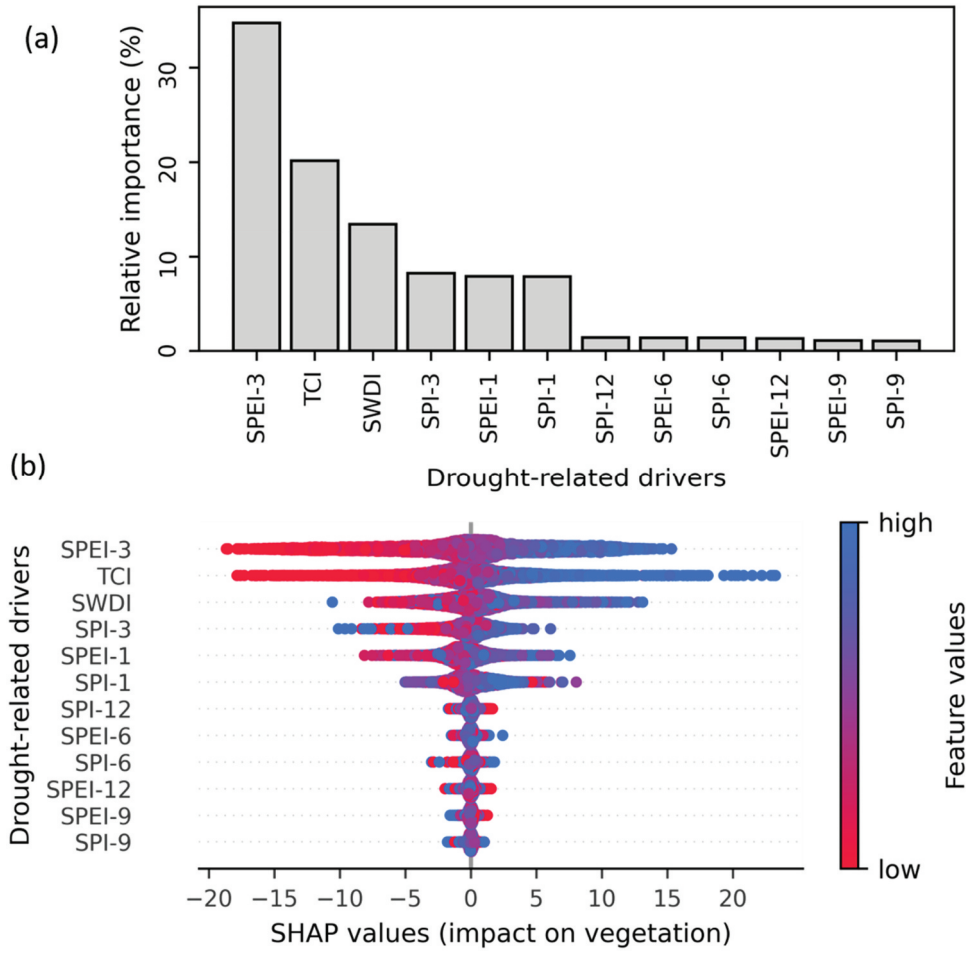

Figure 10. Relative contribution measures of drought impact on vegetation variability across the MSEA region using random forest- and shap-based methods. The bar plot (a) represents the overall importance of driving factors based on SHAP values (in percentage). Higher values indicate more important drivers in random forest and SHAP analyses. The bee swarm plot (b) presents the details of the contribution of individual observations to vegetation dynamics. Positive and negative SHAP values from the bee swarm plot indicate positive (increasing) and negative (decreasing) contributions to vegetation condition while its color bar represents feature observation values from low (drier conditions in red) to high (wetter conditions in blue). The combination of red and blue dots signifies ambiguity in their impact on natural vegetation. Driving factors include the SWDI, SPI, TCI, and SPEI during the dry seasons from 2000 to 2022. To minimize the impact of human activities on vegetation, this analysis is limited to protected areas.

variations, followed by the SWDI (~14%). The SPI-1, SPI-3, and SPEI-1 also has a significant role, collectively accounting for 24% of the variations. By contrast, other drought indices, representing medium and long-term drought conditions, appeared to have a minor impact, accounting for less than 2% in most cases.

Interestingly, it is observed that the TCI can have a considerable influence on natural and undisturbed vegetation in the tropical MSEA region (Figure 10b) in certain cases despite its lower overall importance than the SPEI-3. For example, the wettest condition based on the TCI can increase vegetation up to 25% in some instances, while the driest events can reduce nearly 20% of vegetation. These findings underlined the significance of the thermal temperature variations in influencing natural vegetation dynamics. For instance, Baumbach et al. (2017) reported that European vegetation was significantly vulnerable to extreme temperatures while extreme cold spells substantially reduced vegetation productivity in mid-to-high latitude regions during the spring and summer months (J. Li et al. 2022). Our findings generally agreed with recent studies that tropical vegetation has become more sensitive to extreme temperatures and precipitation (Ciemer et al. 2019; Fan et al. 2023).

Despite the divergent contributions, short-term drought conditions generally had a higher influence on tropical natural vegetation across the MSEA region during dry seasons. This can be attributed to the

responses of natural vegetation to the specific temporal patterns of moisture availability within the ecosystems. For instance, the SPEI-3, considering precipitation and evapotranspiration over a relatively short time (Vicente-Serrano, Beguería, and López-Moreno 2010), aligns closely with the critical period when moisture stress begins to impact tropical vegetation (Chang et al. 2023; Wantong et al. 2022). In arid and semi-arid regions, in comparison, vegetation condition tends to be more sensitive to long-term droughts (Xu et al. 2018; Zhan et al. 2022). In this regard, these findings provide useful information to understand the behaviors of drought conditions that significantly drive natural and undisturbed vegetation changes in the MSEA region. Recognizing the SPEI-3 as the most critical driver has significant implications for understanding and managing natural ecosystem health and vulnerability in these regions. This information enables local land authorities and conservationists to anticipate potential shifts in vegetation distribution and identify areas at higher risk of drought-induced stress. Ultimately, this understanding strengthens the ability to manage and protect tropical ecosystems effectively, providing better guidance for conservation efforts in the face of growing global warming crises.

While the RF regression and SHAP methods can determine the variable importance and provide informative insights into its individual contributions, they may fall short in capturing the full complexity of natural ecosystem responses and interactions. Tropical and subtropical vegetation systems are intricate and influenced by numerous factors, including biotic and abiotic features. Limiting the analysis to drought-related conditions may overlook other crucial drivers, such as wildfires, pest infestations, and forest disturbance. For instance, wildfire events, ignited by a spectrum of natural and human-induced factors, can have profound and immediate effects on vegetation composition and structure (Morresi et al. 2022). Also, the drought indices used in this study were calculated for the duration of the MODIS time series while longer periods (e.g. 30-years) are typically recommended for calculating the SPEI and SPI (Ha et al. 2022; A. K. Mishra and Singh 2010; Vicente-Serrano, Beguería, and López-Moreno 2010). Hence, this problem may influence the reliability of our analysis. It is also important to note that although our analysis is restricted to protected areas and assumes minimal human interference, several studies have reported that the detrimental effects of growing tourism activities and deforestation on natural vegetation and ecosystems within terrestrial protected areas have become more evident in developed and developing countries (Leberger et al. 2020; Pickering and Hill 2007). We acknowledge that protected areas may not cover all natural and undisturbed vegetation ecosystems within the study region. Significant expansions of pristine vegetation may exist beyond protected boundaries, thus warranting consideration despite their exclusion from this study. Last but not the least, there may be discrepancy between the R^2 values on the entire sample dataset and the test data, so the importance of features identified by SHAP values should be interpreted with caution.

Future research endeavors should broaden their scope to encompass diverse drivers, such as El Niño/Southern Oscillation (ENSO), to better understand driving factors in tropical natural vegetation. Given the increasing global warming crisis and significance of tropical biodiversity, this region is expected to experience more intensified and devastating droughts in the foreseeable future, and understanding the sensitivities of vegetation to future drought conditions is crucial for assessing the impacts of climate change on vegetation ecosystems. Thus, simulating and predicting future vegetation-drought sensitivities under different drought scenarios are needed to plan and mitigate the negative effects of climate change on natural ecosystems. Also, the MSEA region consists of interconnected river systems (e.g. Mekong River) and such networks can greatly influence vegetation ecosystems. Hence, network inference analysis should be considered in the future work due to the causal interactions among the eco-hydrological dynamics (J. Li and Convertino 2021; Rinaldo, Gatto, and Rodriguez-Iturbe 2018; H. Wang and Convertino 2023).

Conclusion

The MSEA is a significant region of tropical agriculture and vegetation ecosystems, and has been frequently impacted by severe drought events over the past decades. This study attempted to provide a detailed analysis of vegetation dynamics and their drought impacts using MODIS-based vegetation time series and ensemble of drought indices in consideration of

different land cover types, land-use transitions, and elevation characteristics. Specifically, we first characterized tropical vegetation dynamics and their trends in space and time. Secondly, we assessed vegetation-drought responses using multi-temporal and multi-type drought indices in consideration of land cover and elevation characteristics. Finally, we quantified the drivers and impacts of multifaceted droughts on natural and undisturbed vegetation ecosystem using a robust explainable machine learning method. The main findings of this study are summarized in the following:

- First, the spatiotemporal pattern of vegetation condition and its trend varied across the MSEA region over the past 22 years. Large areas of stressed vegetation were observed during the dry seasons in 2004, 2005, 2010, 2016, 2019, and 2020. Specifically, nearly 80% of the region indicated vegetation stress during the dry season in 2005, while this value amounted to 75% in 2010. This stress was primarily observed in rainfed croplands, especially in Cambodia and Thailand. Despite the temporal variability, a greening trend was observed for almost 70% of the vegetated areas. At country scale, Vietnam had the largest area of greening trend (~75%), followed by Thailand (~70%). By contrast, Cambodia had the largest area of declining vegetation (~60%). These vegetation trends varied with elevation characteristics and land use types, but higher altitudes exhibited a larger greening trend than lower altitudes across land cover types.
- Second, vegetation was highly responsive to drought conditions across the MSEA region, and higher influences of drought were largely found in Myanmar, Thailand, and Cambodia. Generally, vegetation showed a significant positive response ($R = [0.5\text{-}0.75]$) to the drought indices during the dry season. Vegetation had a higher coupling with the TCI among the examined drought indices, and this coupling was found to be stronger with lower elevation in rainfed crop, mixed forest, and deciduous forest. Evergreen forest and irrigated crop vegetation showed the least response to drought indices, especially in high elevation zones.
- Third, short-term drought disturbances accounted for nearly 93% of the variation of the natural and undisturbed tropical vegetation in the MSEA region. The SPEI-3 was identified as the factor having the largest influence among the examined drought indices, explaining approximately 35% of the observed vegetation dynamics, followed by the TCI (~20%). The SPEI-3 indicated that wet conditions can positively alter vegetation condition by up to 15% (in VCI units), while the worst drought events can reduce the vegetation condition up to 20%.

The results of this study deepen the understanding of tropical vegetation variability and how vegetation responds to and is influenced by multifaced drought conditions during the dry growing seasons. The performed in-depth analyses of our study can support local, national, and regional governments to develop effective drought management and adaptation strategies in safeguarding food security and tropical ecosystems. Amidst the growing climate crises, simulating and predicting the future vegetation-drought sensitivities under different drought scenarios will be considered.

Acknowledgments

We acknowledge the DAAD, German Aerospace Center, and Drought-ADAPT project for supporting the open access of this work. Special thanks to Coleman Kjirsten Elizabeth Robyne for English proofreading. We also extend our appreciation to three anonymous reviewers for their valuable comments and feedback, which have significantly enhanced the quality of this manuscript.

Disclosure statement

No potential conflict of interest was reported by the author(s).

Funding

The work was supported by the German Academic Exchange Service.

Data availability statement

This study utilized the following datasets. MODIS data and DEM can be obtainable at NASA's Land Processes Distributed Active Archive Center (http://lpdaac.usgs.gov/) and NASA/

CGIAR (https://srtm.csi.cgiar.org/), respectively. Land cover products are available from ESA CCI (https://www.esa-landcover-cci.org/), and ERA5-Land comes from European Centre for Medium-Range Weather Forecasts (https://www.ecmwf.int/). World Database on Protected Areas are available through Protected Planet (https://www.protectedplanet.net/en). MODIS, DEM, and ERA5-Land can be downloaded through Google Earth Engine.

CRediT authorship contribution statement

Tuyen V. Ha: Conceptualization, Data curation, Methodology, Formal analysis, Visualization, Writing – original draft, Writing – review & editing. **Soner Uereyen**: Writing – review & editing. **Claudia Kuenzer**: Supervision, Conceptualization, Review & editing.

References

AghaKouchak, A., A. Farahmand, F. S. Melton, J. Teixeira, M. C. Anderson, B. D. Wardlow, and C. R. Hain. 2015. "Remote Sensing of Drought: Progress, Challenges and Opportunities." *Reviews of Geophysics* 53 (2): 452–480. https://doi.org/10.1002/2014RG000456.

Allen, R. G., L. S. Pereira, D. Raes, and M. Smith. 1998. "Crop Evapotranspiration-Guidelines for Computing Crop Water Requirements-FAO Irrigation and Drainage Paper 56." *FAO Rome* 300 (9): D05109.

Anderegg, W. R., J. M. Kane, and L. D. Anderegg. 2013. "Consequences of Widespread Tree Mortality Triggered by Drought and Temperature Stress." *Nature Climate Change* 3 (1): 30–36. https://doi.org/10.1038/nclimate1635.

Baumbach, L., J. F. Siegmund, M. Mittermeier, and R. V. Donner. 2017. "Impacts of Temperature Extremes on European Vegetation During the Growing Season." *Biogeosciences* 14 (21): 4891–4903. https://doi.org/10.5194/bg-14-4891-2017.

Beck, H. E., N. E. Zimmermann, T. R. McVicar, N. Vergopolan, A. Berg, and E. F. Wood. 2018. "Present and Future Köppen-Geiger Climate Classification Maps at 1-Km Resolution." *Scientific Data* 5 (1): 1–12. https://doi.org/10.1038/sdata.2018.214.

Berry, P., J. Garlick, and R. Smith. 2007. "Near-Global Validation of the SRTM DEM Using Satellite Radar Altimetry." *Remote Sensing of Environment* 106 (1): 17–27. https://doi.org/10.1016/j.rse.2006.07.011.

Bisquert, M., A. Bégué, M. Deshayes, and D. Ducrot. 2017. "Environmental Evaluation of MODIS-Derived Land Units." *GIScience & Remote Sensing* 54 (1): 64–77. https://doi.org/10.1080/15481603.2016.1256861.

Breiman, L. 2001. "Random Forests." *Machine Learning* 45 (1): 5–32. https://doi.org/10.1023/A:1010933404324.

Cao, S., Y. He, L. Zhang, Q. Sun, Y. Zhang, H. Li, X. Wei, and Y. Liu. 2023. "Spatiotemporal Dynamics of Vegetation Net Ecosystem Productivity and Its Response to Drought in Northwest China." *GIScience & Remote Sensing* 60 (1): 2194597. https://doi.org/10.1080/15481603.2023.2194597.

Cao, S., L. Zhang, Y. He, Y. Zhang, Y. Chen, S. Yao, W. Yang, and Q. Sun. 2022. "Effects and Contributions of Meteorological Drought on Agricultural Drought Under Different Climatic Zones and Vegetation Types in Northwest China." *Science of the Total Environment* 821:153270. https://doi.org/10.1016/j.scitotenv.2022.153270.

Chang, Q., H. He, X. Ren, L. Zhang, L. Feng, Y. Lv, M. Zhang, Q. Xu, W. Liu, and Y. Zhang. 2023. "Soil Moisture Drives the Spatiotemporal Patterns of Asymmetry in Vegetation Productivity Responses Across China." *Science of the Total Environment* 855:158819. https://doi.org/10.1016/j.scitotenv.2022.158819.

Chen, S., P. Olofsson, T. Saphangthong, and C. E. Woodcock. 2023. "Monitoring Shifting Cultivation in Laos with Landsat Time Series." *Remote Sensing of Environment* 288:113507. https://doi.org/10.1016/j.rse.2023.113507.

Ciemer, C., N. Boers, M. Hirota, J. Kurths, F. Müller-Hansen, R. S. Oliveira, and R. Winkelmann. 2019. "Higher Resilience to Climatic Disturbances in Tropical Vegetation Exposed to More Variable Rainfall." *Nature Geoscience* 12 (3): 174–179. https://doi.org/10.1038/s41561-019-0312-z.

Cislaghi, A., L. Giupponi, A. Tamburini, A. Giorgi, and G. B. Bischetti. 2019. "The Effects of Mountain Grazing Abandonment on Plant Community, Forage Value and Soil Properties: Observations and Field Measurements in an Alpine Area." *Catena* 181:104086. https://doi.org/10.1016/j.catena.2019.104086.

Cornish, P. S., C. Birchall, D. F. Herridge, M. D. Denton, and C. Guppy. 2018. "Rainfall-Related Opportunities, Risks and Constraints to Rainfed Cropping in the Central Dry Zone of Myanmar as Defined by Soil Water Balance Modelling." *Agricultural Systems* 164:47–57. https://doi.org/10.1016/j.agsy.2018.04.003.

Cui, T., L. Fan, P. Ciais, R. Fensholt, F. Frappart, S. Sitch, J. Chave, Z. Chang, X. Li, and M. Wang. 2023. "First Assessment of Optical and Microwave Remotely Sensed Vegetation Proxies in Monitoring Aboveground Carbon in Tropical Asia." *Remote Sensing of Environment* 293:113619. https://doi.org/10.1016/j.rse.2023.113619.

Daly, C., M. Halbleib, J. I. Smith, W. P. Gibson, M. K. Doggett, G. H. Taylor, J. Curtis, and P. P. Pasteris. 2008. "Physiographically Sensitive Mapping of Climatological Temperature and Precipitation Across the Conterminous United States." *International Journal of Climatology: A Journal of the Royal Meteorological Society* 28 (15): 2031–2064. https://doi.org/10.1002/joc.1688.

De Jong, R., S. de Bruin, A. de Wit, M. E. Schaepman, and D. L. Dent. 2011. "Analysis of Monotonic Greening and Browning Trends from Global NDVI Time-Series." *Remote Sensing of Environment* 115 (2): 692–702. https://doi.org/10.1016/j.rse.2010.10.011.

De Kauwe, M. G., B. E. Medlyn, A. M. Ukkola, M. Mu, M. E. Sabot, A. J. Pitman, P. Meir, L. A. Cernusak, S. W. Rifai, and B. Choat. 2020. "Identifying Areas at Risk of Drought-Induced Tree Mortality Across South-Eastern Australia." *Global Change*

Biology 26 (10): 5716–5733. https://doi.org/10.1111/gcb.15215.

Didan, K. 2021. "MODIS/Terra Vegetation Indices 16-Day L3 Global 1 Km SIN Grid V061 [Data Set]." *NASA EOSDIS Land Processes DAAC*. Accessed November 15, 2022. https://lpdaac.usgs.gov/products/mod13a2v061/ .

Fan, F., C. Xiao, Z. Feng, and Y. Yang. 2023. "Impact of Human and Climate Factors on Vegetation Changes in Mainland Southeast Asia and Yunnan Province of China." *Journal of Cleaner Production* 415:137690. https://doi.org/10.1016/j.jclepro.2023.137690.

Fang, W., S. Huang, Q. Huang, G. Huang, H. Wang, G. Leng, L. Wang, and Y. Guo. 2019. "Probabilistic Assessment of Remote Sensing-Based Terrestrial Vegetation Vulnerability to Drought Stress of the Loess Plateau in China." *Remote Sensing of Environment* 232:111290. https://doi.org/10.1016/j.rse.2019.111290.

Feng, W., H. Lu, T. Yao, and Q. Yu. 2020. "Drought Characteristics and Its Elevation Dependence in the Qinghai–Tibet Plateau During the Last Half-Century." *Scientific Reports* 10 (1): 14323. https://doi.org/10.1038/s41598-020-71295-1.

Fensholt, R., K. Rasmussen, T. T. Nielsen, and C. Mbow. 2009. "Evaluation of Earth Observation Based Long Term Vegetation Trends—Intercomparing NDVI Time Series Trend Analysis Consistency of Sahel from AVHRR GIMMS, Terra MODIS and SPOT VGT Data." *Remote Sensing of Environment* 113 (9): 1886–1898. https://doi.org/10.1016/j.rse.2009.04.004.

Forzieri, G., V. Dakos, N. G. McDowell, A. Ramdane, and A. Cescatti. 2022. "Emerging Signals of Declining Forest Resilience Under Climate Change." *Nature* 608 (7923): 534–539. https://doi.org/10.1038/s41586-022-04959-9.

Frazier, R. J., N. C. Coops, M. A. Wulder, T. Hermosilla, and J. C. White. 2018. "Analyzing Spatial and Temporal Variability in Short-Term Rates of Post-Fire Vegetation Return from Landsat Time Series." *Remote Sensing of Environment* 205:32–45. https://doi.org/10.1016/j.rse.2017.11.007.

Gessner, U., M. Machwitz, T. Esch, A. Tillack, V. Naeimi, C. Kuenzer, and S. Dech. 2015. "Multi-Sensor Mapping of West African Land Cover Using MODIS, ASAR and TanDEM-X/terraSAR-X Data." *Remote Sensing of Environment* 164:282–297. https://doi.org/10.1016/j.rse.2015.03.029.

Gorelick, N., M. Hancher, M. Dixon, S. Ilyushchenko, D. Thau, and R. Moore. 2017. "Google Earth Engine: Planetary-Scale Geospatial Analysis for Everyone." *Remote Sensing of Environment* 202:18–27. https://doi.org/10.1016/j.rse.2017.06.031.

Göttsche, F.-M., and F. S. Olesen. 2001. "Modelling of Diurnal Cycles of Brightness Temperature Extracted from METEOSAT Data." *Remote Sensing of Environment* 76 (3): 337–348. https://doi.org/10.1016/S0034-4257(00)00214-5.

Goward, S. N., B. Markham, D. G. Dye, W. Dulaney, and J. Yang. 1991. "Normalized Difference Vegetation Index Measurements from the Advanced Very High Resolution Radiometer." *Remote Sensing of Environment* 35 (2–3): 257–277. https://doi.org/10.1016/0034-4257(91)90017-Z.

Grogan, K., D. Pflugmacher, P. Hostert, R. Kennedy, and R. Fensholt. 2015. "Cross-Border Forest Disturbance and the Role of Natural Rubber in Mainland Southeast Asia Using Annual Landsat Time Series." *Remote Sensing of Environment* 169:438–453. https://doi.org/10.1016/j.rse.2015.03.001.

Guo, H., A. Bao, T. Liu, F. Ndayisaba, L. Jiang, A. Kurban, and P. De Maeyer. 2018. "Spatial and Temporal Characteristics of Droughts in Central Asia During 1966–2015." *Science of the Total Environment* 624:1523–1538. https://doi.org/10.1016/j.scitotenv.2017.12.120.

Ha, T. V., J. Huth, F. Bachofer, and C. Kuenzer. 2022. "A Review of Earth Observation-Based Drought Studies in Southeast Asia." *Remote Sensing* 14 (15): 3763. https://doi.org/10.3390/rs14153763.

Ha, T. V., S. Uereyen, and C. Kuenzer. 2023. "Agricultural Drought Conditions Over Mainland Southeast Asia: Spatiotemporal Characteristics Revealed from MODIS-Based Vegetation Time-Series." *International Journal of Applied Earth Observation and Geoinformation* 121:103378. https://doi.org/10.1016/j.jag.2023.103378.

Hamed, K. H., and A. R. Rao. 1998. "A Modified Mann-Kendall Trend Test for Autocorrelated Data." *Journal of Hydrology* 204 (1–4): 182–196. https://doi.org/10.1016/S0022-1694(97)00125-X.

Hansen, M. C., P. V. Potapov, R. Moore, M. Hancher, S. A. Turubanova, A. Tyukavina, D. Thau, S. V. Stehman, S. J. Goetz, and T. R. Loveland. 2013. "High-Resolution Global Maps of 21st-Century Forest Cover Change." *Science* 342 (6160): 850–853. https://doi.org/10.1126/science.1244693.

Hengl, T. 2018. Clay, Sand, and Carbon Organic Contents In% (kg/Kg) at 6 Standard Depths (0, 10, 30, 60, 100 and 200 Cm) at 250 M Resolution. *Zenodo*.

Hersbach, H., B. Bell, P. Berrisford, S. Hirahara, A. Horányi, J. Muñoz-Sabater, and A. Simmons. 2020. "The Era5 Global Reanalysis." *Quarterly Journal of the Royal Meteorological Society* 146 (730): 1999–2049. https://doi.org/10.1002/qj.3803.

Huang, K., and J. Xia. 2019. "High Ecosystem Stability of Evergreen Broadleaf Forests Under Severe Droughts." *Global Change Biology* 25 (10): 3494–3503. https://doi.org/10.1111/gcb.14748.

IPCC. 2013. Climate Change 2013: The Physical Science Basis. Contribution of Working Group I to the Fifth Assessment Report of the Intergovernmental Panel on Climate Change, 1535.

IUCN and UNEP. 2020. *The World Database on Protected Areas (WDPA)*. Cambridge, UK: UNEP-WCMC and IUCN. https://doi.org/10.34892/6fwd-af11.

Jeganathan, C., J. Dash, and P. Atkinson. 2014. "Remotely Sensed Trends in the Phenology of Northern High Latitude Terrestrial Vegetation, Controlling for Land Cover Change and Vegetation Type." *Remote Sensing of Environment* 143:154–170. https://doi.org/10.1016/j.rse.2013.11.020.

Ji, L., and A. J. Peters. 2003. "Assessing Vegetation Response to Drought in the Northern Great Plains Using Vegetation and Drought Indices." *Remote Sensing of Environment* 87 (1): 85–98. https://doi.org/10.1016/S0034-4257(03)00174-3.

Jin, H., S. M. Vicente-Serrano, F. Tian, Z. Cai, T. Conradt, B. Boincean, C. Murphy, B. A. Farizo, S. Grainger, and J. I. López-Moreno. 2023. "Higher Vegetation Sensitivity to Meteorological Drought in Autumn Than Spring Across European Biomes." *Communications Earth & Environment* 4 (1): 299. https://doi.org/10.1038/s43247-023-00960-w.

Kendall, M. G. 1948. *Rank Correlation Methods*. 3rd ed. University of Michigan: Charles Griffin.

Kogan, F. N. 1990. "Remote Sensing of Weather Impacts on Vegetation in Non-Homogeneous Areas." *International Journal of Remote Sensing* 11 (8): 1405–1419. https://doi.org/10.1080/01431169008955102.

Kogan, F. N. 1995. "Application of Vegetation Index and Brightness Temperature for Drought Detection." *Advances in Space Research* 15 (11): 91–100. https://doi.org/10.1016/0273-1177(95)00079-T.

Köppen, W. 1936. "Das geographische System der Klimate." In *Handbuch der Klimatologie*, edited by W. Köppen and R. Geiger, 252. Berlin, Germany: Gebrüder Borntraeger.

Kuenzer, C., P. Leinenkugel, M. Vollmuth, and S. Dech. 2018. "Comparing Global Land-Cover Products–Implications for Geoscience Applications: An Investigation for the Trans-Boundary Mekong Basin." In *Remote Sensing the Mekong*, 6–33. United Kingdom: Routledge.

Lange, M., H. Feilhauer, I. Kühn, and D. Doktor. 2022. "Mapping Land-Use Intensity of Grasslands in Germany with Machine Learning and Sentinel-2 Time Series." *Remote Sensing of Environment* 277:112888. https://doi.org/10.1016/j.rse.2022.112888.

Le, M.-H., H. Kim, H. Moon, R. Zhang, V. Lakshmi, and L.-B. Nguyen. 2020. "Assessment of Drought Conditions Over Vietnam Using Standardized Precipitation Evapotranspiration Index, MERRA-2 Re-Analysis, and Dynamic Land Cover." *Journal of Hydrology: Regional Studies* 32:100767. https://doi.org/10.1016/j.ejrh.2020.100767.

Leberger, R., I. M. Rosa, C. A. Guerra, F. Wolf, and H. M. Pereira. 2020. "Global Patterns of Forest Loss Across IUCN Categories of Protected Areas." *Biological Conservation* 241:108299. https://doi.org/10.1016/j.biocon.2019.108299.

Li, J., E. Bevacqua, C. Chen, Z. Wang, X. Chen, R. B. Myneni, X. Wu, C.-Y. Xu, Z. Zhang, and J. Zscheischler. 2022. "Regional Asymmetry in the Response of Global Vegetation Growth to Springtime Compound Climate Events." *Communications Earth & Environment* 3 (1): 123. https://doi.org/10.1038/s43247-022-00455-0.

Li, J., and M. Convertino. 2021. "Inferring Ecosystem Networks as Information Flows." *Scientific Reports* 11 (1): 7094. https://doi.org/10.1038/s41598-021-86476-9.

Li, Z., T. Huffman, B. McConkey, and L. Townley-Smith. 2013. "Monitoring and Modeling Spatial and Temporal Patterns of Grassland Dynamics Using Time-Series MODIS NDVI with Climate and Stocking Data." *Remote Sensing of Environment* 138:232–244. https://doi.org/10.1016/j.rse.2013.07.020.

Liu, W., and F. Kogan. 1996. "Monitoring Regional Drought Using the Vegetation Condition Index." *International Journal of Remote Sensing* 17 (14): 2761–2782. https://doi.org/10.1080/01431169608949106.

Lloyd-Hughes, B., and M. A. Saunders. 2002. "A Drought Climatology for Europe." *International Journal of Climatology: A Journal of the Royal Meteorological Society* 22 (13): 1571–1592. https://doi.org/10.1002/joc.846.

Lundberg, S. M., and S.-I. Lee. 2017. "A Unified Approach to Interpreting Model Predictions." *Advances in Neural Information Processing Systems* 30. https://doi.org/10.48550/arXiv.1705.07874.

Mann, H. B. 1945. "Nonparametric Tests Against Trend." *Econometrica: Journal of the Econometric Society* 13 (3): 245–259. https://doi.org/10.2307/1907187.

Martínez-Fernández, J., A. González-Zamora, N. Sánchez, and A. Gumuzzio. 2015. "A Soil Water Based Index as a Suitable Agricultural Drought Indicator." *Journal of Hydrology* 522:265–273. https://doi.org/10.1016/j.jhydrol.2014.12.051.

Masson-Delmotte, V., P. Zhai, A. Pirani, S. L. Connors, C. Péan, S. Berger, N. Caud, Y. Chen, L. Goldfarb, and M. Gomis. 2021. Climate Change 2021: The Physical Science Basis. Contribution of Working Group I to the Sixth Assessment Report of the Intergovernmental Panel on Climate Change, 2.

McDowell, N. G., and C. D. Allen. 2015. "Darcy's Law Predicts Widespread Forest Mortality Under Climate Warming." *Nature Climate Change* 5 (7): 669–672. https://doi.org/10.1038/nclimate2641.

McKee, T. B., N. J. Doesken, and J. Kleist. 1993. "The Relationship of Drought Frequency and Duration to Time Scales." In *Proceedings of the 8th Conference on Applied Climatology*, California, USA.

Mishra, A. K., and V. P. Singh. 2010. "A Review of Drought Concepts." *Journal of Hydrology* 391 (1–2): 202–216. https://doi.org/10.1016/j.jhydrol.2010.07.012.

Mishra, A., T. Vu, A. V. Veettil, and D. Entekhabi. 2017. "Drought Monitoring with Soil Moisture Active Passive (SMAP) Measurements." *Journal of Hydrology* 552:620–632. https://doi.org/10.1016/j.jhydrol.2017.07.033.

Morresi, D., R. Marzano, E. Lingua, R. Motta, and M. Garbarino. 2022. "Mapping Burn Severity in the Western Italian Alps Through Phenologically Coherent Reflectance Composites Derived from Sentinel-2 Imagery." *Remote Sensing of Environment* 269:112800. https://doi.org/10.1016/j.rse.2021.112800.

Muñoz-Sabater, J., E. Dutra, A. Agustí-Panareda, C. Albergel, G. Arduini, G. Balsamo, S. Boussetta, M. Choulga, S. Harrigan, and H. Hersbach. 2021. "ERA5-Land: A State-Of-The-Art Global Reanalysis Dataset for Land Applications." *Earth System Science Data* 13 (9): 4349–4383. https://doi.org/10.5194/essd-13-4349-2021.

Nambiar, E. S. 2021. "Strengthening Vietnam's Forestry Sectors and Rural Development: Higher Productivity, Value, and Access to Fairer Markets are Needed to Support Small Forest Growers." *Trees, Forests and People* 3:100052. https://doi.org/10.1016/j.tfp.2020.100052.

Namkhan, M., G. A. Gale, T. Savini, and N. Tantipisanuh. 2021. "Loss and Vulnerability of Lowland Forests in Mainland Southeast Asia." *Conservation Biology* 35 (1): 206–215. https://doi.org/10.1111/cobi.13538.

Naumann, G., C. Cammalleri, L. Mentaschi, and L. Feyen. 2021. "Increased Economic Drought Impacts in Europe with Anthropogenic Warming." *Nature Climate Change* 11 (6): 485–491. https://doi.org/10.1038/s41558-021-01044-3.

Obladen, N., P. Dechering, G. Skiadaresis, W. Tegel, J. Keßler, S. Höllerl, S. Kaps, M. Hertel, C. Dulamsuren, and T. Seifert. 2021. "Tree Mortality of European Beech and Norway Spruce Induced by 2018-2019 Hot Droughts in Central Germany." *Agricultural and Forest Meteorology* 307:108482. https://doi.org/10.1016/j.agrformet.2021.108482.

Palmer, W. C. 1965. *Meteorological Drought*. Vol. 30. United States: US Department of Commerce, Weather Bureau.

Patz, J. A., D. Campbell-Lendrum, T. Holloway, and J. A. Foley. 2005. "Impact of Regional Climate Change on Human Health." *Nature* 438 (7066): 310–317. https://doi.org/10.1038/nature04188.

Pickering, C. M., and W. Hill. 2007. "Impacts of Recreation and Tourism on Plant Biodiversity and Vegetation in Protected Areas in Australia." *The Journal of Environmental Management* 85 (4): 791–800. https://doi.org/10.1016/j.jenvman.2006.11.021.

Qi, C., J. Timmermans, W. Wen, and P. M. van Bodegom. 2023. "Ecosystems Threatened by Intensified Drought with Divergent Vulnerability." *Remote Sensing of Environment* 289:113512. https://doi.org/10.1016/j.rse.2023.113512.

Qin, Y., X. Xiao, J.-P. Wigneron, P. Ciais, M. Brandt, L. Fan, X. Li, S. Crowell, X. Wu, and R. Doughty. 2021. "Carbon Loss from Forest Degradation Exceeds That from Deforestation in the Brazilian Amazon." *Nature Climate Change* 11 (5): 442–448. https://doi.org/10.1038/s41558-021-01026-5.

Qin, Y., X. Xiao, J.-P. Wigneron, P. Ciais, J. G. Canadell, M. Brandt, X. Li, L. Fan, X. Wu, and H. Tang. 2022. "Large Loss and Rapid Recovery of Vegetation Cover and Aboveground Biomass Over Forest Areas in Australia During 2019–2020." *Remote Sensing of Environment* 278:113087. https://doi.org/10.1016/j.rse.2022.113087.

Radanielson, A. M., Y. Kato, L. K. Palao, G. Feyisa, A. J. Malabayabas, J. K. Aunario, C. Garcia, J. G. Balanza, K. T. Win, and R. K. Singh. 2019. "Targeting Management Practices for Rice Yield Gains in Stress-Prone Environments of Myanmar." *Field Crops Research* 244:107631. https://doi.org/10.1016/j.fcr.2019.107631.

Rinaldo, A., M. Gatto, and I. Rodriguez-Iturbe. 2018. "River Networks as Ecological Corridors: A Coherent Ecohydrological Perspective." *Advances in Water Resources* 112:27–58. https://doi.org/10.1016/j.advwatres.2017.10.005.

Rivoire, P., O. Martius, and P. Naveau. 2021. "A Comparison of Moderate and Extreme ERA-5 Daily Precipitation with Two Observational Data Sets." *Earth & Space Science* 8 (4): e2020EA001633. https://doi.org/10.1029/2020EA001633.

Santoro, M., G. Kirches, J. Wevers, M. Boettcher, C. Brockmann, C. Lamarche, and P. Defourny. 2017. *Land Cover CCI: Product User Guide Version 2.0*. Belgium: Climate Change Initiative Belgium.

Seiler, R., F. Kogan, and J. Sullivan. 1998. "AVHRR-Based Vegetation and Temperature Condition Indices for Drought Detection in Argentina." *Advances in Space Research* 21 (3): 481–484. https://doi.org/10.1016/S0273-1177(97)00884-3.

Senf, C., A. Buras, C. S. Zang, A. Rammig, and R. Seidl. 2020. "Excess Forest Mortality is Consistently Linked to Drought Across Europe." *Nature Communications* 11 (1): 6200. https://doi.org/10.1038/s41467-020-19924-1.

Singh, V., and X. Qin. 2020. "Study of Rainfall Variabilities in Southeast Asia Using Long-Term Gridded Rainfall and Its Substantiation Through Global Climate Indices." *Journal of Hydrology* 585:124320. https://doi.org/10.1016/j.jhydrol.2019.124320.

Smith, L. T., L. E. Aragao, C. E. Sabel, and T. Nakaya. 2014. "Drought Impacts on children's Respiratory Health in the Brazilian Amazon." *Scientific Reports* 4 (1): 3726. https://doi.org/10.1038/srep03726.

Son, N. T., C. Chen, C. Chen, L. Chang, and V. Q. Minh. 2012. "Monitoring Agricultural Drought in the Lower Mekong Basin Using MODIS NDVI and Land Surface Temperature Data." *International Journal of Applied Earth Observation and Geoinformation* 18:417–427. https://doi.org/10.1016/j.jag.2012.03.014.

Southworth, J., H. Nagendra, and L. Cassidy. 2012. "Forest Transition Pathways in Asia–Studies from Nepal, India, Thailand, and Cambodia." *Journal of Land Use Science* 7 (1): 51–65. https://doi.org/10.1080/1747423X.2010.520342.

Sun, H., Q. Xu, Y. Wang, Z. Zhao, X. Zhang, H. Liu, and J. Gao. 2023. "Agricultural Drought Dynamics in China During 1982–2020: A Depiction with Satellite Remotely Sensed Soil Moisture." *GIScience & Remote Sensing* 60 (1): 2257469. https://doi.org/10.1080/15481603.2023.2257469.

Tran, T. V., D. Bruce, C.-Y. Huang, D. X. Tran, S. W. Myint, and D. B. Nguyen. 2023. "Decadal Assessment of Agricultural Drought in the Context of Land Use Land Cover Change Using MODIS Multivariate Spectral Index Time-Series Data." *GIScience & Remote Sensing* 60 (1): 2163070. https://doi.org/10.1080/15481603.2022.2163070.

Udelhoven, T., M. Stellmes, G. Del Barrio, and J. Hill. 2009. "Assessment of Rainfall and NDVI Anomalies in Spain (1989–1999) Using Distributed Lag Models." *International Journal of Remote Sensing* 30 (8): 1961–1976. https://doi.org/10.1080/01431160802546829.

UNESCAP. 2019. Asia-Pacific Disaster Report 2019. United Nations Office Bangkok.

Venkatappa, M., N. Sasaki, P. Han, and I. Abe. 2021. "Impacts of Droughts and Floods on Croplands and Crop Production in Southeast Asia–An Application of Google Earth Engine." *Science of the Total Environment* 795:148829. https://doi.org/10.1016/j.scitotenv.2021.148829.

Vicente-Serrano, S. M., S. Beguería, and J. I. López-Moreno. 2010. "A Multiscalar Drought Index Sensitive to Global Warming: The Standardized Precipitation Evapotranspiration Index."

Journal of Climate 23 (7): 1696–1718. https://doi.org/10.1175/2009JCLI2909.1.

Vicente-Serrano, S. M., C. Gouveia, J. J. Camarero, S. Beguería, R. Trigo, J. I. López-Moreno, C. Azorín-Molina, E. Pasho, J. Lorenzo-Lacruz, and J. Revuelto. 2013. "Response of Vegetation to Drought Time-Scales Across Global Land Biomes." *Proceedings of the National Academy of Sciences* 110 (1): 52–57. https://doi.org/10.1073/pnas.1207068110.

Vremec, M., R. A. Collenteur, and S. Birk. 2023. "Improved Handling of Potential Evapotranspiration in Hydrological Studies with PyEt." *Hydrology & Earth System Sciences Discussions* 2023 (417): 1–23. https://doi.org/10.5194/hess-2022-417.

Wan, Z., S. Hook, and G. Hulley. 2021. MOD11A1 MODIS/Terra Land Surface Temperature/Emissivity Daily L3 Global 1km SIN Grid V006. *NASA EOSDIS Land Processes DAAC; 2015*.

Wang, H., A. Chen, Q. Wang, and B. He. 2015. "Drought Dynamics and Impacts on Vegetation in China from 1982 to 2011." *Ecological Engineering* 75:303–307. https://doi.org/10.1016/j.ecoleng.2014.11.063.

Wang, H., and M. Convertino. 2023. "Algal Bloom Ties: Systemic Biogeochemical Stress and Chlorophyll-A Shift Forecasting." *Ecological Indicators* 154:110760. https://doi.org/10.1016/j.ecolind.2023.110760.

Wang, P., E. Asare, V. E. Pitzer, R. Dubrow, and K. Chen. 2022. "Associations Between Long-Term Drought and Diarrhea Among Children Under Five in Low-And Middle-Income Countries." *Nature Communications* 13 (1): 3661. https://doi.org/10.1038/s41467-022-31291-7.

Wang, Y., B. Fu, Y. Liu, Y. Li, X. Feng, and S. Wang. 2021. "Response of Vegetation to Drought in the Tibetan Plateau: Elevation Differentiation and the Dominant Factors." *Agricultural and Forest Meteorology* 306:108468. https://doi.org/10.1016/j.agrformet.2021.108468.

Wantong, L., M. Migliavacca, M. Forkel, J. M. Denissen, M. Reichstein, H. Yang, G. Duveiller, U. Weber, and R. Orth. 2022. "Widespread Increasing Vegetation Sensitivity to Soil Moisture." *Nature Communications* 13 (1): 3959. https://doi.org/10.1038/s41467-022-31667-9.

West, H., N. Quinn, and M. Horswell. 2019. "Remote Sensing for Drought Monitoring & Impact Assessment: Progress, Past Challenges and Future Opportunities." *Remote Sensing of Environment* 232:111291. https://doi.org/10.1016/j.rse.2019.111291.

WMO. 1975. Drought and Agriculture. WMO Technical Note No. 138. Report of the CagM Working Group on the Assessment of Drought. WMO Geneva.

Xu, H.-J., X.-P. Wang, C.-Y. Zhao, and X.-M. Yang. 2018. "Diverse Responses of Vegetation Growth to Meteorological Drought Across Climate Zones and Land Biomes in Northern China from 1981 to 2014." *Agricultural and Forest Meteorology* 262:1–13. https://doi.org/10.1016/j.agrformet.2018.06.027.

Yishan, L., H. Lu, D. Entekhabi, D. J. S. Gianotti, K. Yang, C. Luo, A. F. Feldman, W. Wang, and R. Jiang. 2022. "Satellite-Based Assessment of Meteorological and Agricultural Drought in Mainland Southeast Asia." *IEEE Journal of Selected Topics in Applied Earth Observations & Remote Sensing* 15:6180–6189. https://doi.org/10.1109/JSTARS.2022.3190438.

You, G., Y. Zhang, Y. Liu, D. Schaefer, H. Gong, J. Gao, Z. Lu, Q. Song, J. Zhao, and C. Wu. 2013. "Investigation of Temperature and Aridity at Different Elevations of Mt. Ailao, SW China." *International Journal of Biometeorology* 57 (3): 487–492. https://doi.org/10.1007/s00484-012-0570-6.

Zeng, Z., L. Estes, A. D. Ziegler, A. Chen, T. Searchinger, F. Hua, K. Guan, A. Jintrawet, and F. E. Wood. 2018. "Highland Cropland Expansion and Forest Loss in Southeast Asia in the Twenty-First Century." *Nature Geoscience* 11 (8): 556–562. https://doi.org/10.1038/s41561-018-0166-9.

Zhan, C., C. Liang, L. Zhao, S. Jiang, K. Niu, and Y. Zhang. 2022. "Drought-Related Cumulative and Time-Lag Effects on Vegetation Dynamics Across the Yellow River Basin, China." *Ecological Indicators* 143:109409. https://doi.org/10.1016/j.ecolind.2022.109409.

Zhang, B., F. K. A. Salem, M. J. Hayes, K. H. Smith, T. Tadesse, and B. D. Wardlow. 2023. "Explainable Machine Learning for the Prediction and Assessment of Complex Drought Impacts." *Science of the Total Environment* 898:165509. https://doi.org/10.1016/j.scitotenv.2023.165509.

Zhang, B., L. Zhang, H. Guo, P. Leinenkugel, Y. Zhou, L. Li, and Q. Shen. 2014. "Drought Impact on Vegetation Productivity in the Lower Mekong Basin." *International Journal of Remote Sensing* 35 (8): 2835–2856. https://doi.org/10.1080/01431161.2014.890298.

Zhang, X., and B. Zhang. 2019. "The Responses of Natural Vegetation Dynamics to Drought During the Growing Season Across China." *Journal of Hydrology* 574:706–714. https://doi.org/10.1016/j.jhydrol.2019.04.084.

Zhao, A., A. Zhang, S. Cao, X. Liu, J. Liu, and D. Cheng. 2018. "Responses of Vegetation Productivity to Multi-Scale Drought in Loess Plateau, China." *Catena* 163:165–171. https://doi.org/10.1016/j.catena.2017.12.016.

Zhao, Q., K. Liu, T. Sun, Y. Yao, and Z. Li. 2023. "A Novel Regional Drought Monitoring Method Using GNSS-Derived ZTD and Precipitation." *Remote Sensing of Environment* 297:113778. https://doi.org/10.1016/j.rse.2023.113778.

Zhenzhong, Z., D. Wang, L. Yang, J. Wu, A. D. Ziegler, M. Liu, P. Ciais, T. D. Searchinger, Z.-L. Yang, and D. Chen. 2021. "Deforestation-Induced Warming Over Tropical Mountain Regions Regulated by Elevation." *Nature Geoscience* 14 (1): 23–29. https://doi.org/10.1038/s41561-020-00666-0.

Zoungrana, B. J., C. Conrad, M. Thiel, L. K. Amekudzi, and E. D. Da. 2018. "MODIS NDVI Trends and Fractional Land Cover Change for Improved Assessments of Vegetation Degradation in Burkina Faso, West Africa." *Journal of Arid Environments* 153:66–75. https://doi.org/10.1016/j.jaridenv.2018.01.005.